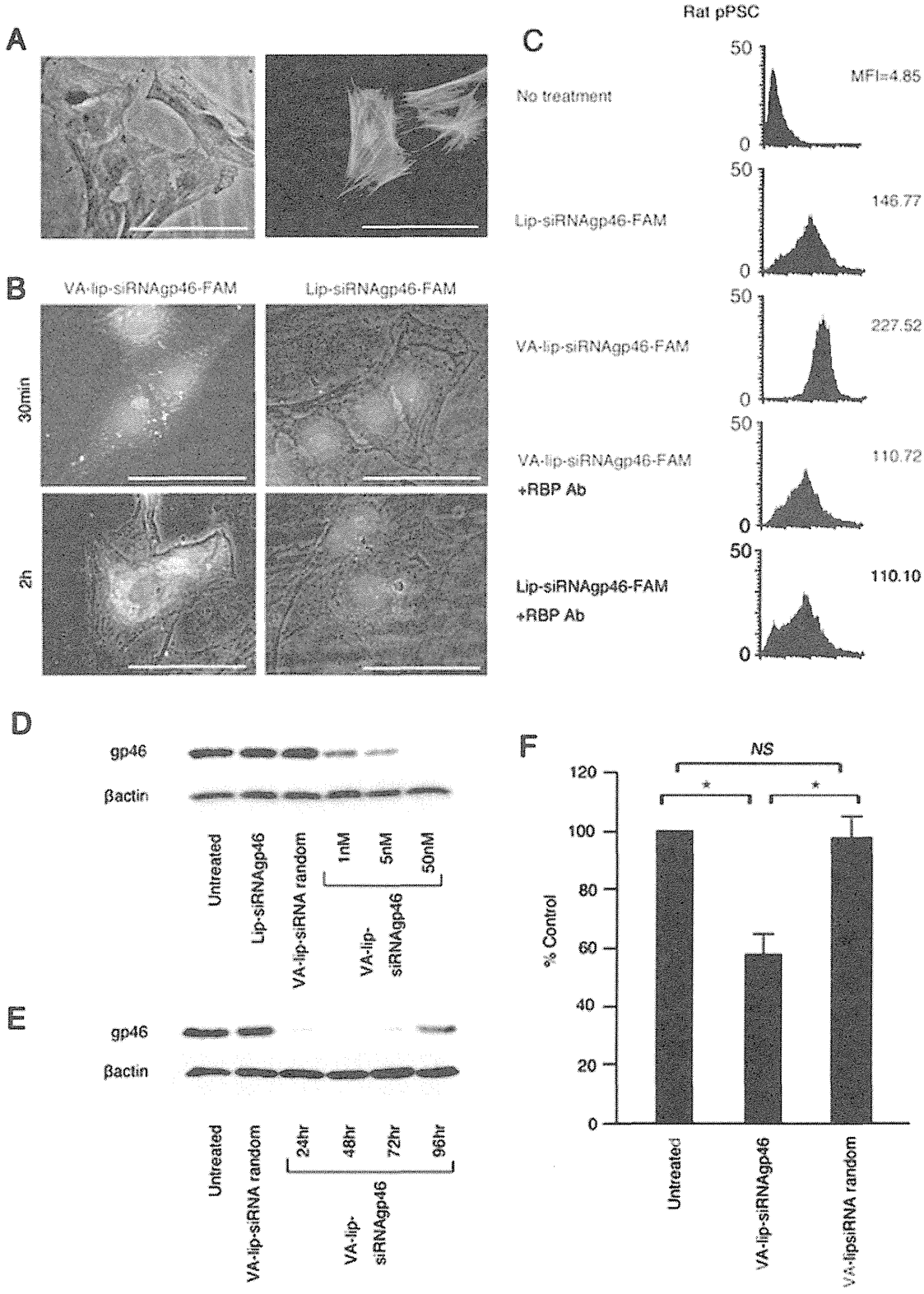

Figure 1 Retinol binding protein receptor-dependent uptake of vitamin A-coupled liposomes (VA-lip-siRNAgp46)-carboxyfluorescein (FAM) by activated pancreatic stellate cells (aPSCs) and suppressive effect of siRNAgp46 on gp46 expression and collagen synthesis. (A) Representative fluorescent images of rat aPSCs. Phase-contrast micrograph image of aPSCs (left panel) and immunofluorescent staining of aPSCs with Cy3-conjugated anti-α-SMA antibody (red) and nuclei counterstained with DAPI (blue) (right panel). Bars=100 μm. (B) Representative fluorescent images of the intracellular distribution of FAM-labelled siRNA. Rat aPSCs were treated with VA-lip-siRNAgp46-FAM or Lip-siRNAgp46-FAM. At 30 min, the medium was replaced with fresh medium. At the time indicated, cells were fixed and analysed by fluorescence microscopy to determine the relative intracellular distribution of siRNA-FAM (green). Bars=100 μm. One of five representative images is shown. (C) Representative fluorescence activated cell sorting patterns of rat PSCs treated with vitamin A-free liposomes carrying siRNAgp46-FAM (Lip-siRNAgp46-FAM) or VA-lip-siRNAgp46-FAM with or without anti-RBP antibody. Mean fluorescence intensity is indicated. Five independent experiments were carried out in each set of aPSCs and the results were essentially the same. (D) Western blotting was used to analyse the expression of gp46 and β-actin

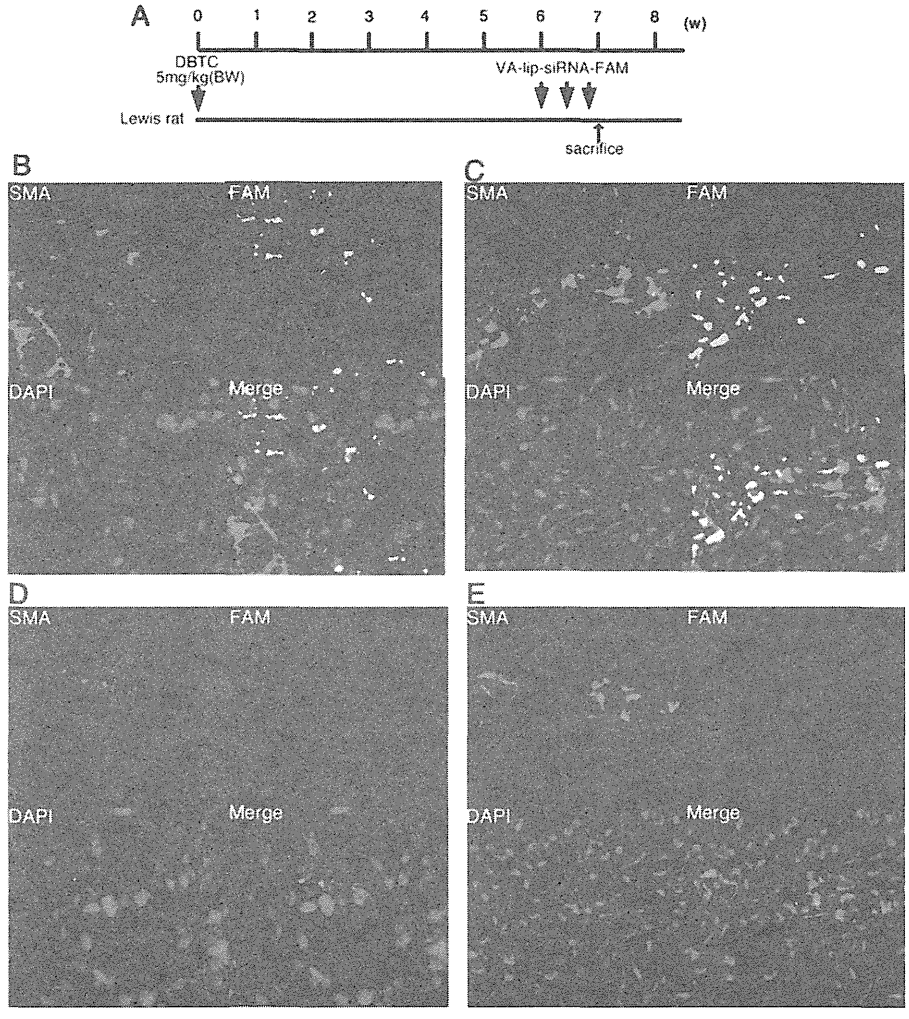

Figure 2 Specific delivery of vitamin A-coupled liposomes(VA-lip-siRNA) random-carboxyfluorescein (FAM) to activated pancreatic stellate cells (aPSCs) in dibutyltin dichloride (DBTC)-treated rats. (A) Schedule of VA-lip-siRNArandom-FAM injection in rats with DBTC-induced pancreatic fibrosis. Samples (B, D; pancreas head, C, E; pancreas body) were obtained from DBTC-treated rats that received three injections of VA-lip-siRNArandom-FAM or Lip-siRNArandom-FAM (siRNA doses of 0.75 mg/kg, 3 times every other day) (n=6 per group). Representative fluorescent images of α-SMA visualised by Cy3-conjugated anti-α-SMA antibody (red), nuclei counterstained with DAPI (blue) and siRNA random-FAM (green) in pancreas specimens obtained 24 h after the last injection. Pictures were taken at original magnification (×200). Fluorescence of siRNA random-FAM (green) was identified in pancreas, predominantly in the region that stained positive for α-SMA giving rise to areas with a merged yellow colour.

spotty region that stained positive only for α-SMA (aPSCs) (red), giving rise to a merged yellow colour (figure 2B,C). By contrast, in rats treated with Lip-siRNArandom-FAM, the yellow area in α-SMA positive regions was negligible (figure 2D,E).

The yellow area in six randomly selected high-power (×200) fields from each specimen occupied 32.1±10.5% of the area stained for α-SMA. By contrast, the yellow area in α-SMA-positive regions was negligible (2.0±1.5%) in a rat injected with lip-siRNAgp46-FAM.

To further elucidate the organ distribution, ^{3}H-labelled VA-lip-siRNArandom was administered to DBTC-treated rats with pancreatitis (day 43) and normal rats (table 1). Radioactivity in the pancreas of DBTC-treated rats was significantly higher (by approximately fivefold) than that of normal rats. In the liver, radioactivity in the DBTC group was also higher (approximately fourfold) than that of normal rats. Other organs, including the lungs, spleen and intestines, showed no increase in radioactivity in DBTC-treated rats, relative to normal rats.

Duration of gp46 suppression in aPSCs in the pancreas of DBTC rats treated with VA-lip-siRNAgp46

To examine the duration of effect of siRNAgp46 on gp46 expression, DBTC rats (n=15) were injected intravenously with VA-lip-siRNAgp46 on day 43 (see online supplementary figure S3A). The expression of gp46 in the pancreas of rats sacrificed at day 43, 44, 45, 46 and 47 (n=3 per group), was analysed by western blotting. The results for each rat per group were essentially the same. Representative western blot bands from one of three rats at each time-point and densitometric values are shown in online supplementary figure S3B,C. Suppression of gp46 expression started 24 h after initiated of treatment and lasted for at least 3 days.

Resolution of pancreatic fibrosis by VA-lip-siRNAgp46 in DBTC-treated rats

After 10 treatments with VA-lip-siRNAgp46 (figure 3A), an apparent reduction and statistically significant reduction analysed by computerised imaging of fibrosis represented by

(normalisation control) in aPSCs transfected with Lip-siRNAgp46,VA-lip-siRNA random or VA-lip-siRNAgp46. Dose-dependent inhibition of gp46 expression by siRNAgp46 was observed. (E) Duration of suppressive effect of siRNAgp46 on gp46 expression in aPSCs. Rat aPSCs were treated with VA-lip-siRNAgp46 or VA-lip-siRNA random. At 30 min, the medium was replaced with fresh medium. At the time indicated, the expression of gp46 and β-actin (normalisation control) was analysed by western blotting. Similar results were obtained in three independent experiments. (F) Collagen deposition on tissue culture plates was assayed by the dye-binding method 72 h after transduction in rat aPSCs treated with VA-lip-siRNAgp46 or with VA-lip-siRNArandom. Data are expressed as mean±SD calculated from five transductions and as a percentage of untreated control. *p<0.05 vs VA-lip-siRNAgp46. NS, not significant.

Table 1 Tissue biodistribution of (^{3}H)VA-lip-siRNAgp46 in rats

	Radioactivity (cpm/tissue)			
	Normal ($\times10^5$)	DBTC rat ($\times10^5$)	p Value (normal vs DBTC rat)	Ratio (DBTC rat/ normal)
Pancreas	0.481±0.270	2.42±0.840	0.001	5.03
Liver	77.2±21.0	319±105	0.002	4.14
Lung	3.83±1.89	5.26±3.66	NS	1.37
Spleen	1.75±0.740	1.84±1.11	NS	1.05
Intestine	4.23±1.59	4.52±1.00	NS	1.07

DBTC-treated rats (day 43 rat) and normal rats (n=3 per group) received a single intravenous injection of 200 μCi (^{3}H)VA-lip-siRNAgp46 via the tail vein. Tissue biodistribution was analysed 24 h later. Data represent means±SD (n=3). Similar results were obtained in two independent experiments.
DBTC, dibutyltin dichloride; NS, not significant; VA-lip-siRNAgp46, vitamin A-coupled liposomes.

Azan-Mallory positive area was confirmed (figure 3B,C). Results were consistent with data showing substantial suppression of hydroxyproline levels (figure 3D).

Disappearance of aPSCs following treatment with VA-lip-siRNAgp46

To elucidate of disappearance of aPSCs after treatment, immunostaining for α-SMA was performed. A substantially smaller area was stained for α-SMA in rats treated with VA-lip-siRNAgp46 compared to the stained area in rats treated with Lip-siRNAgp46 or PBS (figure 3E,F).

Effect of VA-lip-siRNAgp46 treatment on pancreatic inflammation in DBTC-treated rats

Since it is known that PSCs play a role not only in fibrosis but also in the inflammatory response,[21] we explored the effect of VA-lip-siRNAgp46 treatment on inflammation of pancreas in DBTC-treated rats. The degree of inflammation, assessed by cell infiltration, fatty change, tubular complex formation and infiltration of macrophages and T cells were reduced after treatment with VA-lip-siRNAgp46 (see online supplementary figure S4 and table S1).

Resolution of hepatic fibrosis by VA-lip-siRNAgp46 in DBTC-treated rats

In the DBTC model, hepatic fibrosis occurs in addition to pancreatic fibrosis because DBTC causes obstruction of the common bile duct (see online supplementary figure S5A,B). The Azan-Mallory positive area was significantly reduced in specimens from VA-lip-siRNAgp46-treated rats as compared with that in control specimens (see online supplementary figure S5C).

Apoptosis of siRNAgp46-induced aPSCs

We examined the possibility that apoptotic death of rat aPSCs may be induced by siRNAgp46 treatment in vitro. The number of TUNEL positive cells was greater in siRNAgp46-transfected aPSCs than in control aPSCs (figure 4A). The ratio of apoptotic nuclei to total nuclei of siRNAgp46-transfected aPSCs was 38.3±8.2% and was significantly increased relative to controls (figure 4B).

Apoptosis of aPSCs by siRNAHSP47 was also examined in human PSCs obtained by outgrowth from fibrotic human pancreas. TUNEL staining in apoptotic nuclei of siRNAHSP47-transfected aPSCs was higher than in control aPSCs (figure 4C). The ratio of apoptotic nuclei to total nuclei of siRNAHSP47-transfected aPSCs was 18.3±4.2% and was significantly increased relative to controls (figure 4D).

Furthermore, apoptosis of aPSCs by siRNAgp46 was examined in DBTC-treated rats. In DBTC pancreas, TUNEL positive cells in areas overlapping with aPSCs (α-SMA positive) also increased after treatment with VA-lip-siRNAgp46 (figure 4E,F).

Resolution of pancreatic fibrosis by VA-lip-siRNAgp46 in cerulein-treated rats

In the cerulein induced pancreatitis model (see online supplementary figure S2 and figure 5A), the therapeutic effect of VA-lip-siRNAgp46 was also evident with respect to shrinkage of the fibrotic area (figure 5B) and suppression of hydroxyproline levels (figure 5C).

Changes in mRNA expression of fibrosis-related proteins before and after administration of VA-lip-siRNAgp46 in DBTC-treated rats

We measured mRNA levels of gp46, collagen I, MMP2, TIMP-1, and TGFβ in pancreas homogenates from normal rats and DBTC-treated rats (figure 6A). The mRNA ratios relative to GAPDH mRNA are shown in figure 6B. mRNAs of gp46, collagen I, MMP2 and TGFβ expressed in aPSCs were increased in fibrotic pancreas as compared to normal pancreas. TIMP-1 mRNA levels did not increase but instead showed a slight decrease in response to induction of fibrosis. However, after treatment with VA-lip-siRNAgp46, the expression of all mRNAs was significantly decreased, presumably due to the disappearance of aPSCs.

Elevated collagenase activity in the pancreas of DBTC-treated rats

To confirm that sufficient collagenase activity to resolve the predeposited collagen resides in fibrotic pancreas, we measured collagenase activity in the pancreas homogenates of DBTC-treated rats after three injections of VA-lip-siRNAgp46 (day 49), and found that it was significantly higher than that of control normal rat and became even higher after treatment with VA-lip-siRNA gp46 (figure 6C).

Changes in microvessel density in fibrotic pancreas tissue before and after treatment with VA-lip-siRNAgp46

In DBTC-treated pancreas before VA-lip-siRNAgp46 treatment, the mean microvessel counts were 39±9.5. After 10 injections of VA-lip-siRNAgp46, the mean microvessel counts significantly reduced to 19±9.2 (see online supplementary figure S6).

DISCUSSION

PSCs have been shown to store vitamin A and synthesise collagen, and they can be activated by inflammatory cytokines, exerting functions similar to those of HSCs.[1 2 7] However, it has not been elucidated whether RBP is involved in vitamin A uptake. It is also not clear whether HSP47 is involved in collagen secretion by aPSCs. Therefore we first clarified that aPSCs indeed take up vitamin A in an RBP-mediated fashion by demonstrating that with VA-lip-siRNAgp46-FAM, but not with Lip-siRNAgp46-FAM, the fluorescence that appeared within 30 min of incubation was suppressed by anti-RBP antibody, and the amount of collagen on the culture plate of VA-lip-siRNAgp46-treated cells was significantly reduced (figure 1C,F). These findings verified the similarity of aPSCs to activated hepatic stellate cells in terms of RBP-mediated vitamin A uptake and gp46 -assisted collagen secretion.

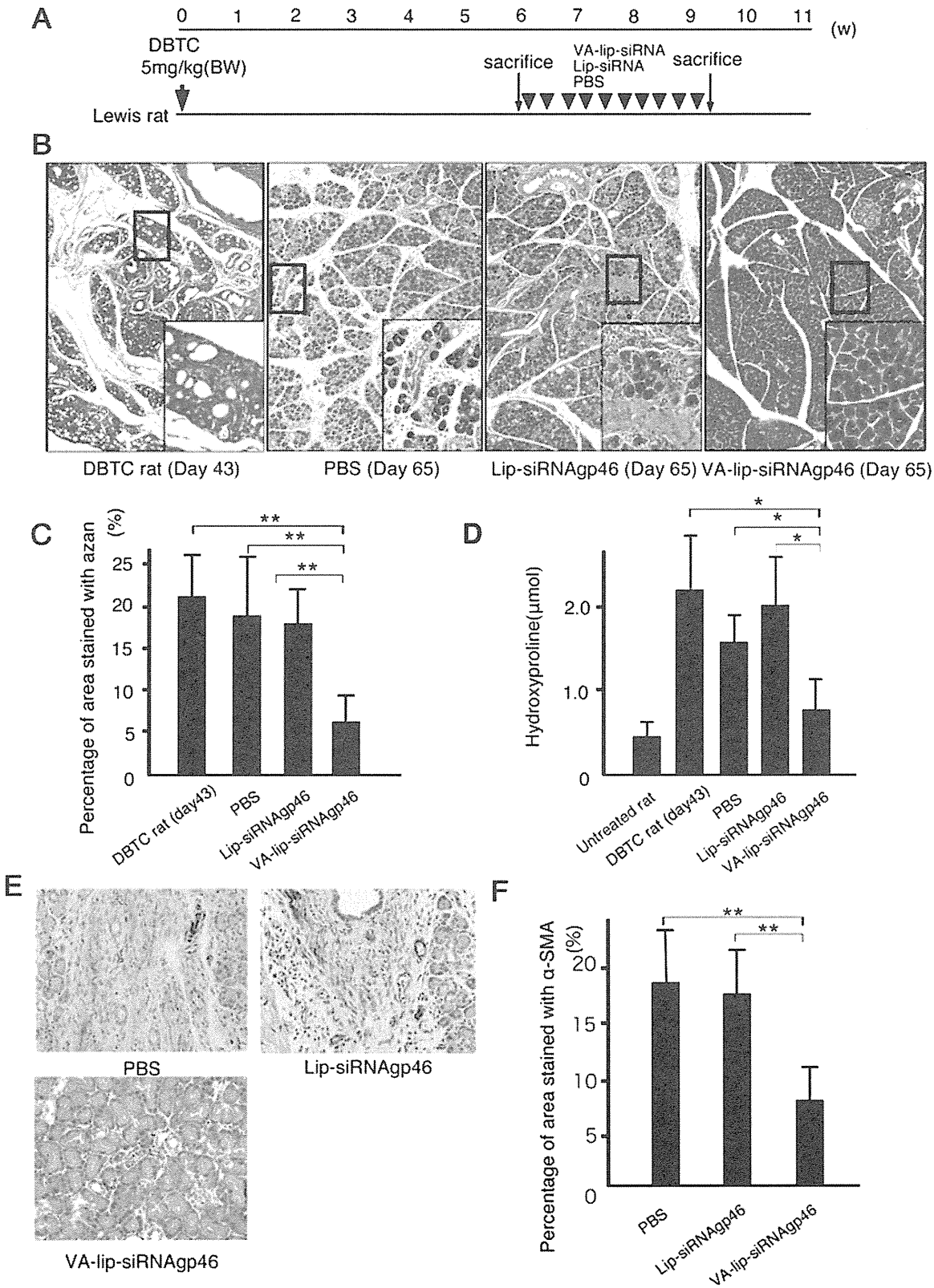

Figure 3 Effect of intravenous injected vitamin A-coupled liposomes (VA-lip-siRNAgp46) on dibutyltin dichloride (DBTC)-induced pancreatic fibrosis. (A) Schedule of VA-lip-siRNAgp46 treatment in rats with DBTC-induced pancreatic fibrosis. Samples were obtained from DBTC-treated rats that received 10 injections of VA-lip-siRNAgp46, Lip-siRNA gp46 (siRNA doses of 0.75 mg/kg, 3 times every other day), or PBS alone (n=10 per group). (B) Representative photomicrographs of Azan-Mallory stained pancreas section. Pictures were taken at original magnification (×100). Magnified images corresponding to the areas enclosed in boxes are presented as indicated. (C) Azan-Mallory positive staining area assessed by computerised image analysis. Data were obtained from six randomly selected fields in each of 10 rats from four groups and represent the mean±SD. (D) Hydroxyproline content in the pancreas. Mean±SD of 10 rats per group. (E) Representative immunohistochemical staining images of activated pancreatic stellate cells stained with anti-α-SMA antibody (brown). Pictures were taken at original magnification (×200). Results from each group of 10 rats were essentially similar. (F) α-SMA-positive staining area assessed by computerised image analysis. Data were obtained from six randomly selected fields in each of 10 rats from three groups and represent the mean±SD. *p<0.05; **p<0.01 vs VA-lip-siRNAgp46 treated- DBTC rat.

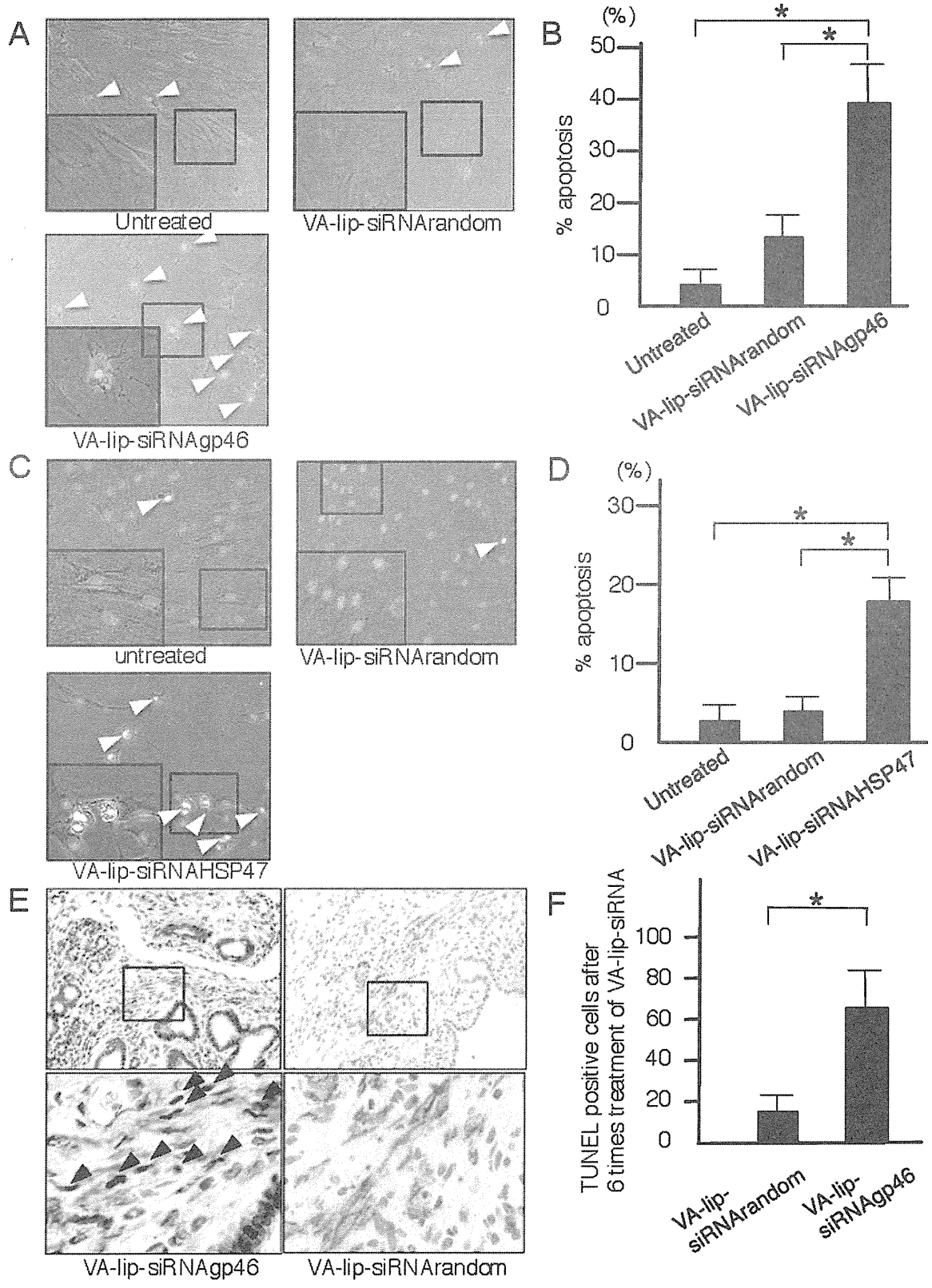

Figure 4 Apoptosis of activated pancreatic stellate cells (aPSCs) induced by vitamin A-coupled liposomes (VA-lip-siRNA) treatment. (A) Representative photomicrographs of rat aPSCs undergoing apoptosis. Nuclei of aPSCs treated with VA-lip-siRNAgp46 or with control agents were stained with FITC-transferase-mediated deoxyuridine triphosphate nick-end labelling (TUNEL) (green) and DAPI (blue) 72 h after each treatment. Arrowheads indicate apoptotic cells. Pictures taken at original magnification (×200) and magnified images corresponding to the areas enclosed in boxes are presented in the inset. (B) Quantification of apoptotic aPSCs shown in figure 4A. Apoptotic nuclei (green) and total nuclei (green + blue) were examined by fluorescent microscopy and counted in 10 randomly selected fields per slide for each indicated treatment; the ratios of apoptotic to normal nuclei were expressed as percentages. Results represent the mean±SD of three independent experiments. *$p<0.01$ vs VA-lip-siRNAgp46. (C) Representative photomicrographs of human aPSCs undergoing apoptosis. Nuclei of aPSCs treated with VA-lip-siRNAHSP47 or with control agents were stained with FITC-TUNEL (green) and DAPI (blue) 72 h after each treatment. Arrowheads indicate apoptotic cells. Pictures taken at original

Incidentally, regarding a possible role of other cellular components such as myofibroblasts in pancreatic fibrosis, it is rather difficult to distinguish it from that of aPSCs since when PSCs are activated, they become positive for α-SMA, which is characteristic of myofibroblasts. In this context, it should be noted that quiescent PSCs store vitamin A, and when they become myofibroblasts, although no more vitamin A droplets in their cytoplasm are observed, they still can take up vitamin A as shown by in vitro transfection experiments using VA-lip-siRNAgp46. This was true for hepatic stellate cells too. This is carefully discussed in our previous paper.[6] It is speculated that deposited vitamin A in quiescent cells may be used up or partly excreted on myofibrobrast transformation.

Prior to the examination of therapeutic effect, we assured specific delivery of VA-lip-siRNAgp46 to aPSCs in fibrotic pancreas tissue, demonstrating the mergence of the green fluorescence of siRNA-FAM encapsulated in vitamin A liposomes with the red fluorescence of α-SMA-positive cells (aPSCs), and higher accumulation of ^{3}H-VA-lipsiRNA in the pancreas of DBTC-treated rats than that in normal rats. The reason for 10-fold more radioactivity in the lung and intestine may be due to the higher content of macrophages in these organs. However, the 150-fold difference between liver and pancreas may not be simply ascribed to the difference in macrophage content, but more likely to the increased number of activated hepatic stellate cells since in this model, not only pancreas but also liver undergoes fibrosis because of obstruction of the common bile duct.

Collectively these results supported the notion that aPSCs preferentially take up siRNAgp46 encapsulated in vitamin A liposomes in vivo. We also examined the kinetics of the effect in vivo, prior to assessment of therapeutic efficacy, and found that the suppression of gp46 expression lasted for 3 days after the injection of VA-lip-siRNAgp46. Thus, our therapy protocol involved injecting the drug three times per week.

The therapeutic effect of treatment, namely, histological improvement and normalised hydroxyproline levels in the pancreas, was observed following administration of drug 10 times. In our previous study using liver cirrhosis models, substantial resolution of fibrotic tissue was obtained after only five treatments.[6] In the present study, we also initially used only five treatments, but improvement of fibrosis was unsatisfactory. This may be due to the fact that the pancreas is relatively poor in blood supply compared with the liver, and thus the dosage of siRNAgp46 at the fibrotic loci supplied by five injections may not have been sufficient to bring about effective resolution of pancreatic fibrosis.

Incidentally, it may be noteworthy to mention that our treatment brought about less vessel density since it promises wider implications such as depletion of tumour stroma in pancreas cancer. In this regard, it is nowadays a well accepted concept that modality to normalise the vascularity by diminishing immature microvessels with anti-neoangiogenesis antibody, rather enhances the efficacy of chemotherapy when the antibody and anticancer drug are used in combination.[22]

Regarding the mechanism for the enhanced microvascularity in fibrotic tissue and decrement of vascularity after treatment, we assume, in good agreement with reports by and Hideshima and Okada,[23 24] that aPSCs are producing angiogenesis factor(s) which will be eradicated from the tissue in accordance with apoptosis induction by treatment. This assumption is based on our recent finding that rat aPSCs are indeed expressing some angiogenesis factors, including fibroblast growth factor (unpublished observation).

The resolution of fibrosis appears to occur by a dual mechanism involving siRNAgp46, which inhibits de novo secretion of collagen, and tissue collagenase, which dissolves predeposited collagen matrix. This assumption is consistent with the fact that collagenase activity in the pancreas at day 42 and day 49 after DBTC treatment, when massive fibrosis occurred, was higher than that of normal pancreas. The reason for sustained high collagenase activity after VA-lip-siRNAgp46 treatment, despite the suppressed MMP2 mRNA, may be that TIMP from aPSCs is also reduced due to apoptosis of aPSCs. In addition, a persistent extracellular matrix pool of collagenase after it is secreted from cells may account for the sustained collagenase activity.[25 26] Activation of matrix metalloproteinases (MMPs) derived from inflammatory cells by reduced TIMP-1 expression may also account for the discrepancy.

Furthermore, apoptosis of aPSCs via transduction of siRNAgp46 was confirmed in our vitro experiment, indicating that a similar mechanism is involved in apoptosis of aHSCs and aPSCs. It is plausible that collagen secreted by aHSCs and aPSCs serves as a survival signal and that this signal is abrogated, leading to apoptosis, as a result of collagen degradation by collagenase (unpublished observation). In support of this possibility, our results demonstrated that high collagenase activity was maintained in the pancreas even after treatment (figure 6C). Incidentally, induction of apoptosis by inhibiting collagen secretion was confirmed to occur even in human PSCs treated with VA-lip-siRNAHSP47, indicating applicability of this approach in the clinical setting.

Interestingly, inflammation associated with fibrosis in this model was also decreased by this treatment, probably due to the fact that aPSCs, which were eradicated by our treatment, are involved not only in the development of fibrosis but also in the inflammatory reaction.[21]

Liver fibrosis in DBTC-treated rats was also successfully resolved with treatment in the present study. However, because the epithelial plug in the common duct was not removed by the treatment, increased serum amylase, alanine aminotransferase and bilirubin persisted (data not shown). In the DBTC

magnification (×200) and magnified images corresponding to the areas enclosed in boxes are presented in the inset. (D) Quantification of apoptotic aPSCs shown in figure 4C. Apoptotic nuclei (green) and total nuclei (green + blue) were examined by fluorescent microscopy and counted in 10 randomly selected fields per slide for each indicated treatment; the ratios of apoptotic to normal nuclei were expressed as percentages. Results represent the mean±SD of three independent experiments. *p<0.01 vs VA-lip-siRNAHSP47. (E) Representative immunohistochemical staining of pancreas specimens from dibutyltin dichloride (DBTC) (5 mg/kg) treated rats (day 56) that received six injections of VA-lip-siRNAgp46 (left panel) or VA-lip-siRNArandom (right panel) (siRNA doses of 0.75 mg/kg, 3 times every other day) stained for TUNEL (brown, arrowhead) and α-SMA (red). Magnified images of the corresponding areas in boxes indicated that the number of cells with TUNEL-positive overlapping of α-SMA-positive PSCs was substantially increased in VA-lip-siRNAgp46 specimens compared with VA-lip-siRNArandom specimens. Pictures were taken at original magnification (×100). (F) Quantification of TUNEL-positive PSCs in pancreas specimens from VA-lip-siRNAgp46-treated DBTC-rats and VA-lip-siRNArandom. The number of TUNEL-positive cells in α-SMA-positive areas was counted in 10 randomly selected fields per pancreas section of each rat. *p<0.01. The results were essentially similar within each group of three rats.

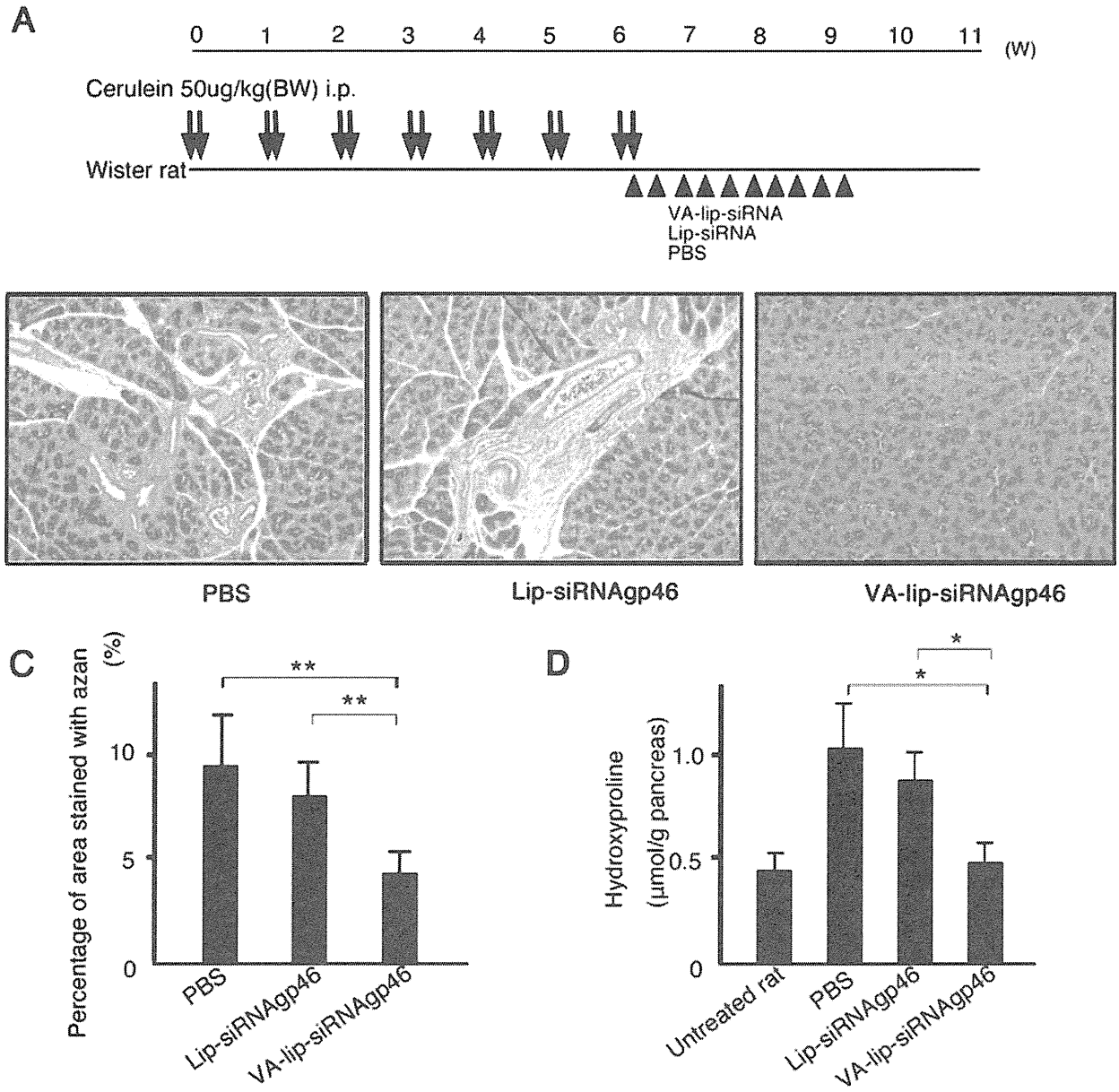

Figure 5 Effect of intravenous injected vitamin A-coupled liposomes (VA-lip-siRNAgp46) on cerulein-induced pancreatic fibrosis. (A) Schedule of VA-lip-siRNAgp46 treatment in rats with cerulean-induced pancreatic fibrosis. Samples were obtained from cerulean-treated rats that received 10 injections of VA-lip-siRNAgp46, Lip-siRNA gp46 (siRNA doses of 0.75 mg/kg, 3 times every other day) or PBS alone (n=10 per group). (B) Representative photomicrographs of an Azan-Mallory-stained pancreas section. Pictures taken at original magnification (×100). (C) Azan-Mallory-positive staining area assessed by computerised image analysis. Data were obtained from six randomly selected fields in each of 10 rats from three groups and represent the mean±SD. (D) Hydroxyproline content in the pancreas. Mean±SD of 10 rats per group. *p<0.05; **p<0.01 vs VA-lip-siRNAgp46 treated-dibutyltin dichloride rat.

model, unlike in advanced chronic pancreatitis in humans, β-cells remained intact and, therefore, no change in blood glucose levels was observed throughout the experimental period (data not shown).

To further evaluate the therapeutic effect of our modality in another model, we established a chronic pancreatitis model based on repeated administration of cerulein to rats.[12 18] The results in this model were compatible with those of the DBTC model, confirming the general efficacy of our modality in dissimilar pancreatic fibrosis models.

Off-target effects and stimulation of toll-like receptors (TLRs) are both critical issues to be solved in the application of therapies using siRNA. Since we used the same siRNA as that of the previous study on liver cirrhosis in which we denied a bystander effect by demonstrating comparable gene silencing efficacy and antifibrotic effect with two other independent siRNAs against the same target,[6] we believe it is unlikely to be the case.

Nonetheless, for future clinical applications, it will be necessary to conduct careful explorations of adverse effects, off-target effects and TLR stimulation.

In conclusion, the present data clearly indicate the therapeutic potential of our modality for pancreas fibrosis and suggest its potential for the treatment of organ fibrosis.

Contributors HI, YS and KM designed research, performed experiments and wrote the paper. AY, RF, HN, NB, TH, TS, KM, RT, MK, SA, YK, KH and JK performed experiments. YN designed research, wrote the paper and supervised the whole project. All authors discussed the results and commented on the manuscript.

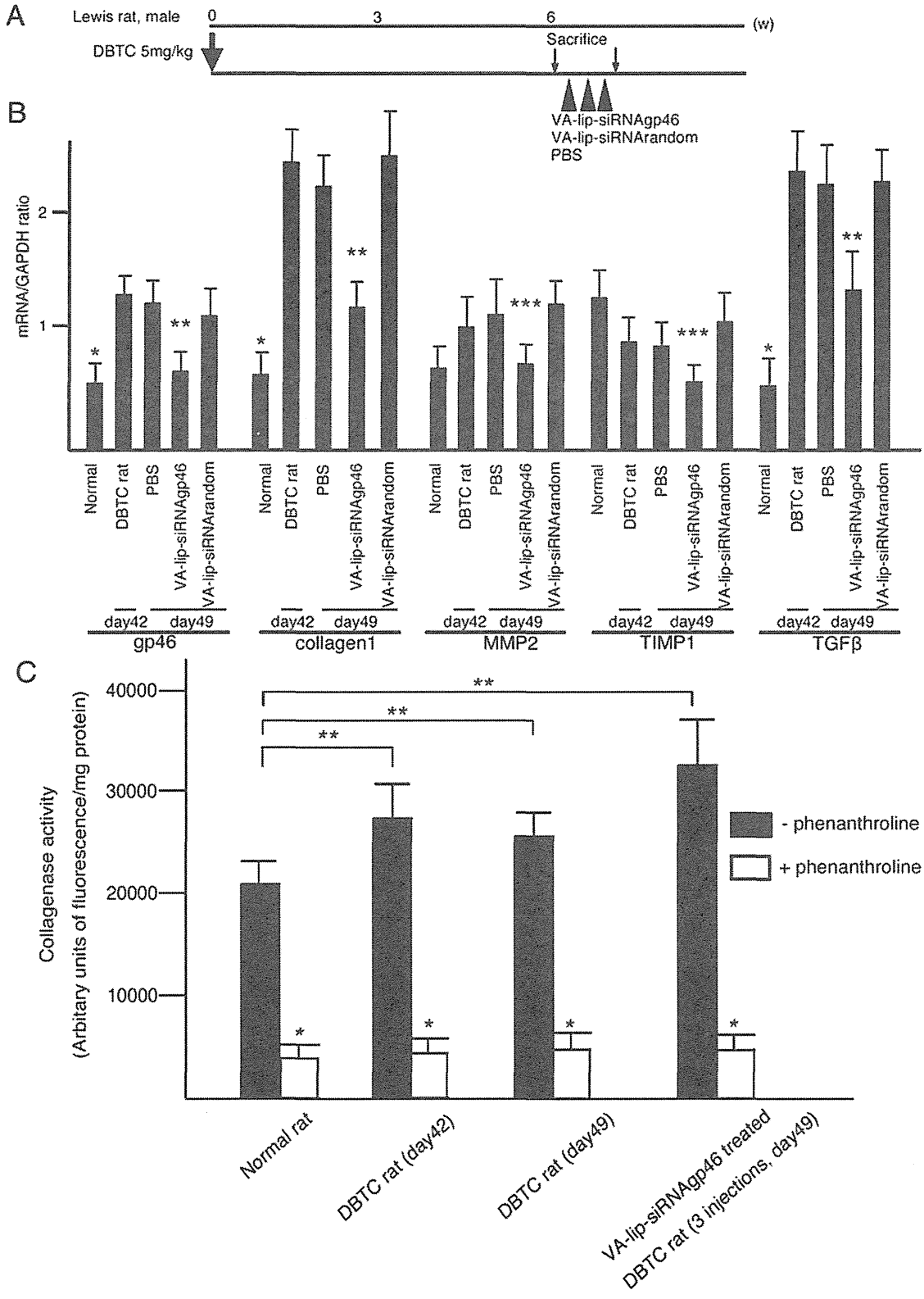

Figure 6 Effect of vitamin A-coupled liposomes (VA-lip-siRNAgp46) treatments on mRNA expression of fibrosis-related proteins and collagenase activity in pancreas homogenates. (A) Schedule of VA-lip-siRNAgp46 treatment in rats with dibutyltin dichloride (DBTC)-induced pancreatic fibrosis. Samples were obtained from DBTC-treated rats that received three injections of VA-lip-siRNAgp46, Lip-siRNA gp46 (siRNA doses of 0.75 mg/kg, 3 times every other day), or PBS alone (n=3 per group). (B) The expression of gp46, procollagen I, MMP-2, TIMP-1, and TGFβ mRNA in normal rats, DBTC-treated rats treated with three injections of PBS, DBTC-treated rats treated with three injections of VA-lip-siRNArandom, and DBTC-treated rats treated with three injections of VA-lip-siRNAgp46 were quantitated by real-time PCR. Expression was normalised as the ratio to GAPDH mRNA, a housekeeping gene. *p<0.01 vs DBTC rat (day42). **p<0.01 vs PBS (day46). ***p<0.05 vs PBS (day46). (C) Total collagenase activity in pancreas homogenates from normal rats, DBTC-treated rats (day 42), DBTC-treated rats (day 49), and DBTC rats treated with three injections of VA-lip-siRNAgp46 (siRNA doses of 0.75 mg/kg, 3 times every other day, day 49) in the absence or presence of MMP inhibitor (1,10-phenanthroline). Results are the mean±SD of five rats per group. *p<0.01 vs without inhibitor. **p<0.05 vs normal rat.

Competing interests None.

Provenance and peer review Not commissioned; externally peer reviewed.

REFERENCES

1. **Bachem MG,** Schneider E, Gross H, *et al*. Identification, culture, and characterization of pancreatic stellate cells in rats and humans. *Gastroenterology* 1998;**115**:421–32.
2. **Schneider E,** Schmid-Kotsas A, Zhao J, *et al*. Identification of mediators stimulating proliferation and matrix synthesis of rat pancreatic stellate cells. *Am J Physiol Cell Physiol* 2001;**281**:C532–43.
3. **Shimizu K,** Shiratori K, Kobayashi M, *et al*. Troglitazone inhibits the progression of chronic pancreatitis and the profibrogenic activity of pancreatic stellate cells via a PPARgamma-independent mechanism. *Pancreas* 2004;**29**:67–74.
4. **Yamada T,** Kuno A, Masuda K, *et al*. Candesartan, an angiotensin II receptor antagonist, suppresses pancreatic inflammation and fibrosis in rats. *J Pharmacol Exp Ther* 2003;**307**:17–23.
5. **Kuno A,** Yamada T, Masuda K, *et al*. Angiotensin-converting enzyme inhibitor attenuates pancreatic inflammation and fibrosis in male Wistar Bonn/Kobori rats. *Gastroenterology* 2003;**124**:1010–19.
6. **Sato Y,** Murase K, Kato J, *et al*. Resolution of liver cirrhosis using vitamin A-coupled liposomes to deliver siRNA against a collagen-specific chaperone. *Nat Biotechnol* 2008;**26**:431–42.
7. **Buchholz M,** Kestler HA, Holzmann K, *et al*. Transcriptome analysis of human hepatic and pancreatic stellate cells: organ-specific variations of a common transcriptional phenotype. *J Mol Med* 2005;**83**:795–805.
8. **Apte MV,** Haber PS, Applegate TL, *et al*. Periacinar stellate shaped cells in rat pancreas: identification, isolation, and culture. *Gut* 1998;**43**:128–33.
9. **Williams EJ,** Benyon RC, Trim N, *et al*. Relaxin inhibits effective collagen deposition by cultured hepatic stellate cells and decreases rat liver fibrosis in vivo. *Gut* 2001;**49**:577–83.
10. **Inoue M,** Ino Y, Gibo J, *et al*. The role of monocyte chemoattractant protein-1 in experimental chronic pancreatitis model induced by dibutyltin dichloride in rats. *Pancreas* 2002;**25**:e64–70.
11. **Merkord J,** Jonas L, Weber H, *et al*. Acute interstitial pancreatitis in rats induced by dibutyltin dichloride (DBTC): pathogenesis and natural course of lesions. *Pancreas* 1997;**15**:392–401.
12. **Elsasser HP,** Haake T, Grimmig M, *et al*. Repetitive cerulein-induced pancreatitis and pancreatic fibrosis in the rat. *Pancreas* 1992;**7**:385–90.
13. **Puig-Divi V,** Molero X, Salas A, *et al*. Induction of chronic pancreatic disease by trinitrobenzene sulfonic acid infusion into rat pancreatic ducts. *Pancreas* 1996;**13**:417–24.
14. **Merkord J,** Weber H, Jonas L, *et al*. Influence of ethanol on long-term effects of dibutyltin dichloride (DBTC) in pancreas and liver of rats. *Hum Exp Toxicol* 1998;**17**:144–50.
15. **Yamamoto M,** Otani M, Otsuki M. A new model of chronic pancreatitis in rats. *Am J Physiol Gastrointest Liver Physiol* 2006;**291**:G700–8.
16. **Tsuchitani M,** Saegusa T, Narama I, *et al*. A new diabetic strain of rat (WBN/Kob). *LabAnim* 1985;**19**:200–7.
17. **Sparmann G,** Merkord J, Jaschke A, *et al*. Pancreatic fibrosis in experimental pancreatitis induced by dibutyltin dichloride. *Gastroenterology* 1997;**112**:1664–72.
18. **Ishibashi T,** Zhao H, Kawabe K, *et al*. Blocking of monocyte chemoattractant protein-1 (MCP-1) activity attenuates the severity of acute pancreatitis in rats. *J Gastroenterol* 2008;**43**:79–85.
19. **Iredale JP,** Benyon RC, Pickering J, *et al*. Mechanisms of spontaneous resolution of rat liver fibrosis. Hepatic stellate cell apoptosis and reduced hepatic expression of metalloproteinase inhibitors. *J Clin Invest* 1998;**102**:538–49.
20. **Weidenbach H,** Lerch MM, Turi S, *et al*. Failure of a prolyl 4-hydroxylase inhibitor to alter extracellular matrix deposition during experimental pancreatitis. *Digestion* 1997;**58**:50–7.
21. **Masamune A,** Watanabe T, Kikuta K, *et al*. Roles of pancreatic stellate cells in pancreatic inflammation and fibrosis. *Clin Gastroenterol Hepatol* 2009;**7**:S48–54.
22. **Jain RK.** Normalizing tumor vasculature with anti-angiogenic therapy: a new paradigm for combination therapy. *Nat Med* 2001;**7**:987–9.
23. **Hideshima K,** Seike J, Mimura S, *et al*. HSP47 and angiogenic factor expression and its implication for the healing of periosteal defects in the mouse cranium. *Oral Med Pathol* 2006;**11**:27–33.
24. **Okada H,** Inoue T, Kanno Y, *et al*. Selective depletion of fibroblasts preserves morphology and the functional integrity of peritoneum in transgenic mice with peritoneal fibrosing syndrome. *Kidney Int* 2003;**64**:1722–32.
25. **Zhou X,** Hovell CJ, Pawley S, *et al*. Expression of matrix metalloproteinase-2 and -14 persists during early resolution of experimental liver fibrosis and might contribute to fibrolysis. *Liver Int* 2004;**24**:492–501.
26. **Steffensen B,** Wallon UM, Overall CM. Extracellular matrix binding properties of recombinant fibronectin type II-like modules of human 72-kDa gelatinase/type IV collagenase. High affinity binding to native type I collagen but not native type IV collagen. *J Biol Chem* 1995;**270**:11555–66.

Zoledronic Acid But Not Somatostatin Analogs Exerts Anti-Tumor Effects in a Model of Murine Prostatic Neuroendocrine Carcinoma of the Development of Castration-Resistant Prostate Cancer

Kohei Hashimoto,[1] Naoya Masumori,[1]* Toshiaki Tanaka,[1] Toshihiro Maeda,[1] Ko Kobayashi,[1] Hiroshi Kitamura,[1] Koichi Hirata,[2] and Taiji Tsukamoto[1]

[1]*Department of Urology, Sapporo Medical University School of Medicine, Japan*
[2]*First Department of Surgery, Sapporo Medical University School of Medicine, Japan*

BACKGROUND. Since neuroendocrine (NE) cells play an important role in the development of castration-resistant prostate cancer (CRPC), target therapy to NE cells should be considered for treating CRPC. We investigated the effects zoledronic acid (ZOL) and two somatostatin analogs (octreotide: SMS, and pasireotide: SOM) on an NE allograft (NE-10) and its cell line (NE-CS), which were established from the prostate of the LPB-Tag 12T-10 transgenic mouse.

METHODS. We examined the in vivo effects of ZOL, SMS and SOM as single agents and their combinations on subcutaneously inoculated NE-10 allografts and the in vitro effects on NE-CS cells. Apoptosis and cell cycle activity were assessed by immunohistochemistry using TdT-mediated dUTP-biotin nick-end labeling (TUNEL) and a Ki-67 antibody, respectively.

RESULTS. In vivo growth of NE-10 tumors treated with ZOL, ZOL plus SMS, or ZOL plus SOM was significantly inhibited compared to the control as a consequence of induction of apoptosis and cell cycle arrest. ZOL induced time- and dose-dependent inhibition of in vitro proliferation of NE-CS cells, but the somatostatin analogs (SMS and SOM) did not. ZOL also inhibited migration of NE-CS cells. These effects were caused by inhibition of Erk1/2 phosphorylation via impairment of prenylation of Ras.

CONCLUSIONS. ZOL, but not SMS or SOM, induced apoptosis and inhibition of proliferation and migration through impaired prenylation of Ras in NE carcinoma models. Our findings support the possibility that ZOL could be used in the early phase for controlling NE cells, which may trigger progression to CRPC. *Prostate* © 2012 Wiley Periodicals, Inc.

KEY WORDS: **zoledronic acid; somatostatin analog; neuroendocrine carcinoma; prostate cancer; anti-tumor effect**

INTRODUCTION

Prostate cancer is the most common noncutaneus malignancy in men in developed countries [1]. Its incidence has been gradually increasing even in non-Caucasian men. As the growth of cancer cells is androgen-dependent, androgen deprivation therapy including surgical or chemical castration has been the mainstay of treatment for advanced prostate cancer. The response to this treatment lasts for a median of 36–48 months [2]. However, in most cases, the disease progresses despite the castration level of serum testosterone, and results in castration-resistant prostate cancer (CRPC). The prognosis of CRPC is poor and a concrete treatment strategy has not yet been established.

*Correspondence to: Naoya Masumori, Department of Urology, Sapporo Medical University School of Medicine S1, W16, Chuo-ku, Sapporo 060-8543, Japan. E-mail: masumori@sapmed.ac.jp
Received 4 June 2012; Accepted 27 August 2012
DOI 10.1002/pros.22590
Published online in Wiley Online Library (wileyonlinelibrary.com).

The exact mechanisms behind progression to castration resistance remain poorly understood. However, recent studies suggest that neuroendocrine (NE) cells, as well as pathways involving or bypassing the androgen receptor (AR), may play an important role in the development of castration resistance [3]. NE cells are present in both the normal and neoplastic prostate. They regulate surrounding prostate cells by secreting growth-modulating neuropeptides such as chromogranin A, serotonin and parathyroid hormone-related protein (PTHrP) [4]. Increases in the NE phenotype and secretory products are thought to be closely associated with progression and castration resistance in prostate cancer [5,6]. Previously, we developed an NE allograft (NE-10) and its cell line (NE-CS) from the prostate of the LPB-Tag 12T-10 transgenic mouse [7–9]. We demonstrated that secretions from NE cells induced androgen-independent growth of human prostate cancer cell line LNCaP and promoted pulmonary metastasis [10]. Therefore, it is crucial to seek a new drug or drug combinations targeting these prostatic NE carcinoma models (NE-10 and NE-CS).

Zoledronic acid (ZOL) is a nitrogen-containing bisphosphonate that inhibits bone resorption of osteoclasts through the inhibition of farnesyl-pyrophosphate synthetase in the mevalonate pathway. This agent has been demonstrated to have beneficial effects in patients with bone metastases of prostate cancer, reducing bone pain and skeletal-related events [11]. ZOL was also shown to have direct anti-tumor activity in several cancer cell lines. It is suggested that ZOL inhibits proliferation and induces apoptosis by impairment of prenylation of Ras and other small GTP-binding proteins (G proteins) [12].

Somatostatin is a peptide hormone that regulates secretion of various exocrine and endocrine glands via specific somatostatin receptors (SSTR). Five different subtypes (SSTR1-5), which are coupled to G proteins, have been identified [13]. Since a majority of NE tumors predominantly express SSTR2, somatostatin analogs having high affinity for SSTR2a such as octreotide (SMS) are considered to be drugs for NE tumors [14,15]. Since several studies have reported that SSTR1 and SSTR5 are expressed in addition to SSTR2 in prostate cancer tissue [15,16], new somatostatin analogs such as pasireotide (SOM) that have high affinity for SSTR5 in addition to SSTR2 [17], may be useful as new drugs for prostatic NE carcinoma.

In the present study, we investigated whether the growth of NE carcinoma models (NE-10, NE-CS) could be influenced by ZOL and/or somatostatin analogs (SMS and SOM), having potential anti-tumor activities.

MATERIALS AND METHODS

Cell Lines and Lell Culture

NE-CS is a murine prostate neuroendocrine cancer cell line established in our institute [9]. It was derived from an NE-10 tumor [8]. Passage numbers between 12, and 16 were used in the study. The NE-CS cells were maintained in the culture medium described below in 5% CO_2 in a humidified incubator. The medium consisted of RPMI-1640 (Gibco BRL, Breda, The Netherlands) that was supplemented with MEM nonessential amino acid (10 ml/L, Gibco BRL), MEM sodium pyruvate, penicillin–streptomycin (10 ml/L, Gibco BRL), 10% fetal bovine serum (FBS, ICN Biomedicals, Costa Mesa, CA), and 7.5% $NaHCO_3$.

ReverseTranscription Polymerase Chain Reaction (RT-PCR) Analysis

To investigate expression of SSTR in NE-10, RT-PCR analysis was performed. Tumor tissues in allografts of NE-10 were homogenized. Total RNA was extracted using an RNeasy kit (Qiagen, Valencia, CA) according to the manufacturer's instructions. A total of 2 μg of total RNA was reverse transcribed in a thermal cycles (Perkin–Elmer, Norwalk, CT) using SuperScript III (Invitrogen, Carlsbad, CA) and oligo (dT) 12–18 primers according to the manufacturer's instructions for 1 hr at 50°C in a 40 μl reaction mixture. Resulting cDNA (1 μl) was amplified with Taq polymerize and one set of oligonucleotide primers. Samples were denatured for 5 min at 94°C, and then amplified for 35 cycles at 94°C for 30 sec, 57°C for 30 sec, and 72°C for 1 min. Aliquots (9 μl) from each PCR sample were then analyzed by agarose-gel electrophoresis. Forward and reverse primer sequences were as follows: SSTR2a (5′-CAGCTGTACCATCAACTGGC, 5′-ATTTGTCCTGCTTACTGTCG), SSTR2b (5′-TGATCAATGTAGCTGTGTGG, 5′-CAAAGAACATTCTGGAAGC), SSTR5 (5′-TGCCTGATGGTCATGAGTGT, 5′-GGAAACTCTGGCGGAAGTTA), GAPDH (5′-TACAGCAACAGGGTGGTGGA, 5′-ACCACAGTCCATGCCATCAC).

Growth of NE-10 Allografts In Vivo

To examine the in vivo effects of ZOL, SMS and SOM as single agents and their combinatorial effects on prostatic NE carcinoma, we used NE-10 allografts. Six-week-old male BALB/c nude mice were castrated using the scrotal approach. After one week, 50 mg tissue fragments of the NE-10 allograft were inoculated subcutaneously (s.c.) into the flanks of mice. Two weeks after transplantation, NE-10 tumors grew to a volume of more than 100 mm^3. The mice were then

randomized into six treatment groups (13 mice in each group): ZOL, SMS, SOM, ZOL plus SMS, ZOL plus SOM, and control. The groups were treated for 6 weeks with ZOL (1 μg/mouse, three times per week, s.c.), SMS (2 μg/mouse, once per day, s.c.), SOM (2 μg/mouse, twice per day, s.c.), ZOL plus SMS (1 μg/mouse, three times per week, s.c. plus 2 μg/mouse, once per day, s.c.), ZOL plus SOM (1 μg/mouse, three times per week, s.c. plus 2 μg/mouse, twice per day, s.c.), or saline (an equal volume of solvent/day, s.c.). These substances were dissolved in 100 μl saline. ZOL, SMS, and SOM were kindly provided by Novartis Pharma AG (Basel, Switzerland). These agents were soluble in saline. The body weights of mice were measured each week. The effects of treatments on tumor growth were determined by measuring tumor volume ($0.523 \times \text{long diameter}^2 \times \text{short diameter}$). After 6 weeks of treatment, the mice were killed and the tumor and liver were removed. Liver weight was measured, and the numbers of metastatic nodules on the liver surface were macroscopically counted. The tissues were fixed in 10% formalin and embedded in paraffin. The 5 μm thick paraffin-embedded material was routinely processed for hematoxylin and eosin staining.

The Animal Experiment Committee of Sapporo Medical University approved the in vivo experiments. Animal care and housing followed the guidelines of the Animal Experiment Committee.

Cell Cycle and Apoptosis Analysis of Tissue Sections

Immunohistochemical staining was done with formalin-fixed paraffin-embedded tissue sections of NE-10 tumors. The 5 μm thick sections were deparaffinized in xylene and rehydrated in graded alcohol. Antigen retrieval was done by boiling sections for 20 min in a microwave oven in preheated 0.01 mol/L sodium citrate buffer (pH 6.0). Endogenous peroxidase activity was blocked by 3% hydrogen peroxide in ethanol for 10 min. After blocking with 1% non-fat dry milk in phosphate-buffered saline (PBS) (pH 7.4), the sections were reacted with a rabbit polyclonal anti-Ki-67 antibody (Abcam plc., Cambridge, UK) at 20 μg/ml or preimmune sera for 1 hr, followed by incubation with biotinylated goat anti-rabbit IgG (Nichirei, Tokyo, Japan) for 30 min. Subsequently, the sections were stained with streptavidin-biotin complex (Nichirei), followed by incubation with 3,3-diaminobenzidine and counterstaining with hematoxylin. The same tissues were immunostained by TdT-mediated dUTP-biotin nick-end labeling (TUNEL) (In situ Apoptosis Detection Kit, Takara Bio, Inc., Otsu, Japan). The Ki-67 labeling index (KI) and apoptotic index (AI) were determined as the ratios of immunohistochemically positive cells per 1,000 NE cells by using a fluorescence microscope (model BZ-9000; Keyence, Osaka, Japan).

Proliferation Assays

NE-CS cells (1 × 104) were suspended with 100 μl of culture medium in a 96-well plate for 24 hr, and then treated with the indicated concentrations (from 0.1 to 100 μmol/L) of ZOL, SMS and SOM for 24, 48, or 72 hr. For combination, the same concentrations of ZOL and SMS or SOM were used; for example, 1 μmol/L of ZOL to 1 μmol/L of SMS. In addition, they were treated with the indicated concentrations (from 0.1 to 100 μmol/L) of ZOL plus 1, 5, and 20 μmol/L of farnesyl-pyrophosphate ammonium salt (FOH) (Sigma–Aldrich, St. Louis, MO) for 48 hr. FOH is an isoprenoid to be involved in prenylation of several G proteins including Ras in the intracellular mevalonate pathway. Cell proliferation was assessed using a WST-8 (modified tetrazolium salt) cell proliferation kit (Cell Counting Kit-8, Dojin, Japan). Changes in absorbance at 450 nm were measured with a microplate reader. The growth inhibition was determined as the concentration inducing 50% inhibition (IC50). For analysis of the synergism between ZOL and somatostatin analogs (SMS and SOM), the combination indices (CI) were calculated by the isobologram equation method [18,19], and CI values of <1, 1, and >1 were considered to indicate synergistic, additive, and antagonistic effects, respectively 12.

Cell Cycle and Apoptosis Assays

NE-CS cells (3 × 104) were suspended with 100 μl of culture medium in a 96-well plate for 24 hr, and then treated with various concentrations of ZOL (from 10 to 100 μmol/L) for 48 hr. Then the cells were fixed with 4% paraformaldehyde, permeabilized with 0.1% Triton X-100, and labeled with the TUNEL technique (In situ Cell Death Detection Kit TMR red, Roche Diagnostics, Mannheim, Germany) and the primary anti-Ki-67 antibody at a 1/200 dilution (Abcam plc., Cambridge, UK). The Ki-67 antibody was detected with an Alexa Fluor 488 donkey anti-rabbit antibody, and nuclei were stained with 4,6-diamidino-2-phenylindole (DAPI) (Invitrogen, Carlsbad, CA). As in the in vivo study, the KI and the AI were measured by fluorescence immunohistochemistry using a fluorescence microscope (model BZ-9000; Keyence, Osaka, Japan).

Migration Assays

Cell migration analyses were performed as described previously (10). In a trans-well culture

chamber (Coster Science, Cambridge, MA), a polyvinylpyrrolidone-free polycarbonate filter with an 8.0 μm pore size was precoated with 5 μg of fibronectin (Biomedical Technologies, Stoughton, MA) on the lower surface. Two different experiments were performed. In experiment 1, NE-CS cells (1×10^5) were placed in the upper chamber with 100 μl of culture medium with or without ZOL (10, 100 μmol/L). In the lower chamber, 600 μl of culture medium was added. In experiment 2, NE-CS cells (1×10^5) were placed in the upper chamber with 100 μl of culture medium adding 20 μmol/L of FOH with or without ZOL (10, 100 μmol/L). In the lower chamber, 600 μl of culture medium was added. The cells that migrated across the pores at 2, 4, 6, and 8 hr were counted under a microscope after hematoxylin and eosin staining. The experiments were carried out in triplicate. Data are shown as number of cells 1 mm^{-2} of membrane.

Pull Down and Western Blot Assays

NE-CS cells (1×10^5) were suspended with 2 ml of culture medium in a 6-well plate for 24 hr, and then treated with ZOL (10, 100 μmol/L) or ZOL (10, 100 μmol/L) + 20 μmol/L FOH for 48 hr. Subsequent to the treatment, cells were washed three times with ice-cold PBS and solubilized in lysis buffer [RIPA buffer, 100 mmol/L PMSF, 500 mmol/L Na_3VO_4, 1 mol/L NaF, 2 mol/L Sigma 104 phosphatase substrate, Protease Inhibitor Mini Cocktail]. The total protein content of the cell lysates was determined by the BCA Protein Assay (Pierce, Rockford, IL).

Activated Ras was detected by pull-down assay. The GTP-bound form of Ras in the cell lysates was affinity-purified using the Raf1-Ras-binding domain (RBD)-GST complexed with glutathione beads following the manufacturer's instructions (Active Ras Pull Down and Detection Kit, Thermo Fisher Science, Waltham, MA). Complexes were analyzed by SDS–PAGE and immunobloting with a Ras-specific antibody.

The cells lysates obtained were boiled in SDS sample buffer containing 0.5 mol/L 2-mercaptoethanol. Samples were separated by SDS–PAGE, transferred to polyvinylidene difluoride (PVDF) membranes and immunoblotted with rabbit monoclonal anti-Erk1/2 and anti-phospho-Erk1/2 antibodies (Cell Signaling Technology Inc., MA), and a mouse monoclonal anti-β-actin antibody (Sigma–Aldrich). Separated proteins were visualized using horseradish peroxidase with enhancement by chemiluminescence (GE Healthcare Bio-Sciences Corp., NJ).

Statistical Analysis

We used the computer program StatView 5.0 for Windows (SAS Institute, Cary, NC). Student's *t*-test was applied to compare results between two different groups. Repeated-measures ANOVA was used when comparing the in vivo tumor volume, and the in vitro cell migration in an individual group. One-way ANOVA was used when comparing the in vivo apoptosis, cell cycle progression, and liver metastases in an individual group. Statistical significance was assigned at $P < 0.05$.

RESULTS

Expression of SSTR2a and SSTR5 in NE-10 Allografts

Since effects of somatostatin analogs are mediated by expression of SSTR, we examined expression of the somatostatin receptor subtypes SSTR2 and SSTR5, to which SMS and SOM preferentially bind, respectively. Gene expression of SSTR2a and SSTR5 was observed in NE-10 allografts, but that of SSTR2b was not (Fig. 1).

Effects of ZOL, SMS and SOM as Single Agents and in Combination on Subcutaneously Inoculated NE-10 Allografts

Growth of NE-10 tumors in mice treated with ZOL, ZOL plus SMS, and ZOL plus SOM was significantly slowed compared to the saline control ($P = 0.003$, $P < 0.001$, and $P = 0.001$, respectively) (Fig. 2A). All treatments were well tolerated with maintenance of body weight (data not shown). We examined whether anti-tumor effects of each treatment were induced by apoptosis or cell cycle arrest by using TUNEL and Ki67 staining, respectively (Fig. $2B_1$). The AI was significantly increased in tumors of mice treated with ZOL, ZOL plus SMS, or ZOL plus SOM compared to the control (means: 9.2, 11.6, and 12.7, respectively, vs. 2.4) (Fig. $2B_2$). The KI was significantly decreased in tumors of mice treated with ZOL, ZOL plus SMS, or ZOL plus SOM compared to the control (means: 5.3, 8.3, and 4.2, respectively, vs. 15.9) (Fig. $2B_3$). The

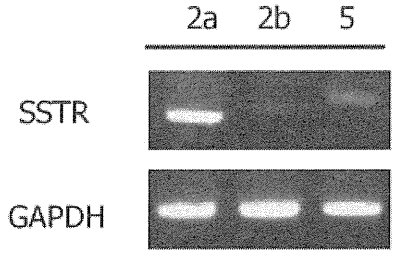

Fig. 1. Expression of SSTR2a, SSTR2b, and SSTR5 in NE-10 allograft by RT-PCR. Gene expression of SSTR2a, and SSTR5 was observed in the NE-10 allograft, but that of SSTR2b was not.

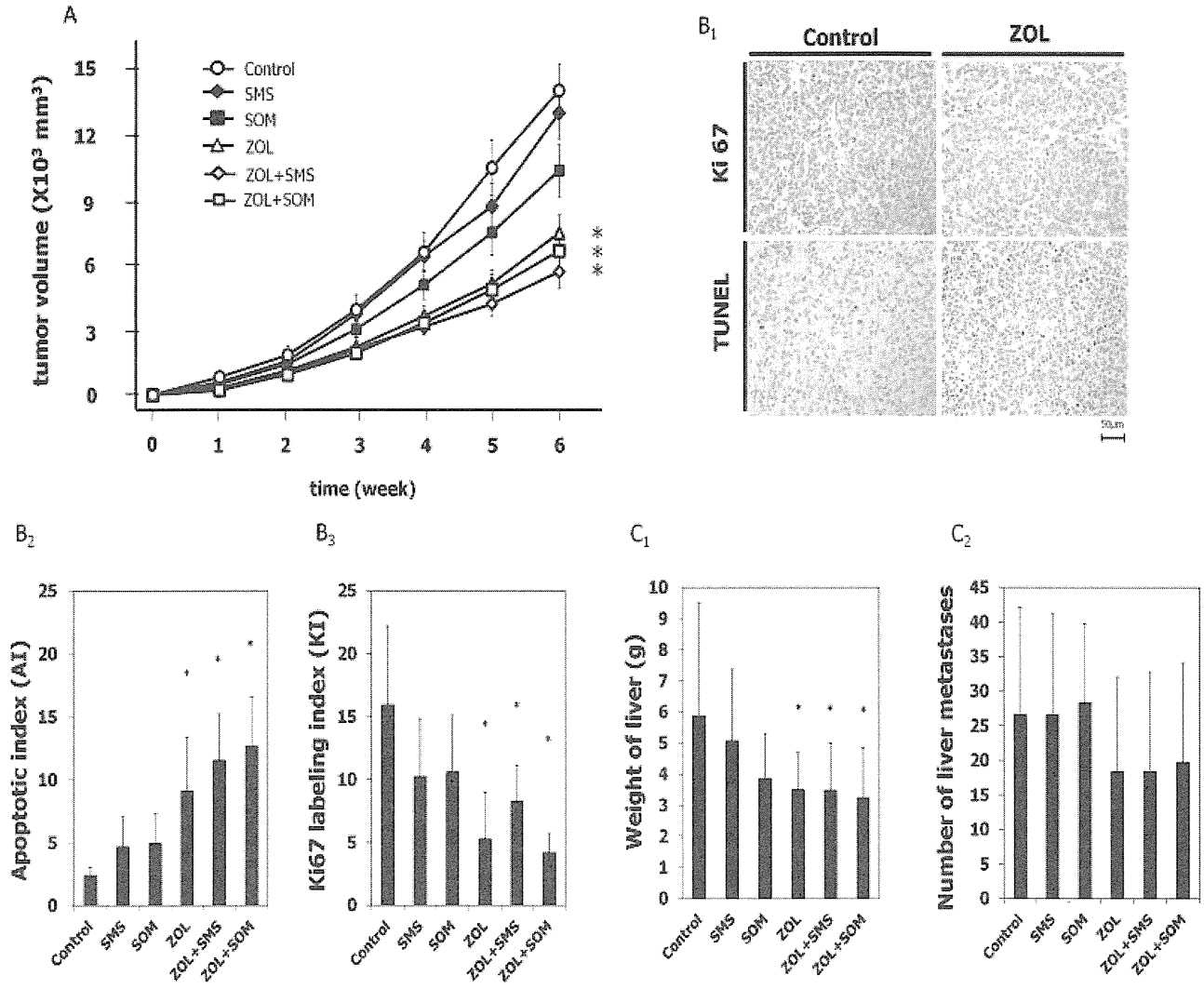

Fig. 2. Effects of ZOL, SMS, and SOM as single agents and in combination on subcutaneous inoculated NE-10 allografts. Six-week-old male BALB/c nude mice were castrated. After one week, 50 mg tissue fragments from the NE-10 allograft model were subcutaneously inoculated into the backs of mice. For 2 weeks, NE-10 tumors were allowed to grow to approximately more than 100 mm^3 before randomization into six treatment groups: control, ZOL, SMS, SOM, ZOL plus SMS, and ZOL plus SOM (n = 13/group). NE-10 allografts in each group were treated for 6 weeks. **A**: Growth of NE-10 tumors in mice treated with ZOL, ZOL plus SMS, and ZOL plus SOM was significantly slowed compared to the saline control ($P = 0.003$, $P < 0.001$, and $P = 0.001$, respectively). Data are means; bars ± SE; *, significantly different from control group ($P < 0.05$; repeated-measures ANOVA). **B**: Effects of ZOL, SMS and SOM as single agents and in combination on apoptosis and cell cycle progression. Immunohistochemical staining was done by using TUNEL and Ki67 staining (**B_1**). Apoptoic effects were measured by the number of TUNEL-positive cells per 1,000 cells, apoptoic index (AI). The AI was significantly increased in tumors from mice treated with ZOL, ZOL plus SMS, or ZOL plus SOM compared to the control (means: 9.2, 11.6, and 12.7, respectively, vs. 2.4) (**B_2**). Cell cycle progression was measured by the number of Ki67-positive cells per 1,000 cells (KI: Ki-67 labeling index). The KI was significantly decreased in tumors from mice treated with ZOL, ZOL plus SMS, or ZOL plus SOM compared to the control (means: 5.3, 8.3, and 4.2, respectively, vs. 15.9) (**B_3**). Data are means; bars ± SD; *, significantly different from control group ($P < 0.05$; one-way ANOVA). **C**: Effects of ZOL, SMS and SOM as single agents and in combination on liver metastases. The weights of livers having metastatic nodules in ZOL, ZOL plus SMS, or ZOL plus SOM were significantly lower than for the control (**C_1**). The numbers of metastatic nodules in these groups were not significantly different from the control (**C_2**). Data are means; bars ± SD. *, Significantly different from control group ($P < 0.05$; one-way ANOVA).

weights of livers having metastatic nodules in ZOL, ZOL plus SMS, or ZOL plus SOM were significantly lower than for the control (Fig. $2C_1$), but the numbers of metastatic nodules in these groups were not significantly different from the control (Fig. $2C_2$).

Effects of ZOL, SMS and SOM as Single Agents and in Combination on Growth of NE-CS Cells In Vitro

We investigated the inhibitory effects of ZOL, SMS, and SOM, alone and in combination on proliferation

of NE-CS cells. Cell viability was measured by the WST-8 assay when NE-CS cells were treated with various concentrations of ZOL, SMS and SOM (0.1–100 μmol/L) in the treatment groups for 24, 48 or 72 hr. For combinations, the same concentrations of ZOL and SMS or SOM were used. The IC50 for ZOL at 72 hr was 15.7 μmol/L, whereas those for ZOL plus SMS, and ZOL plus SOM were 14.1, and 13.5 μmol/L, respectively (Fig. 3A). The combination of ZOL and somatostatin analogs did not demonstrate synergistic effects (CI: 0.57–1.00). ZOL induced time- and dose-dependent proliferative inhibition of NE-CS cells (Fig. 3B). These effects of ZOL were reversed by 20 μmol/L of FOH (Fig. 3C).

ZOL Inhibits Cell Cycle Activity and Induces Apoptosis of NE-CS Cells

TUNEL-positive cells, indicated in red, increased with increased concentrations of ZOL. On the other hand, Ki-67-positive cells, colored green, decreased (Fig. 4A). We also analyzed the AI and KI with ZOL

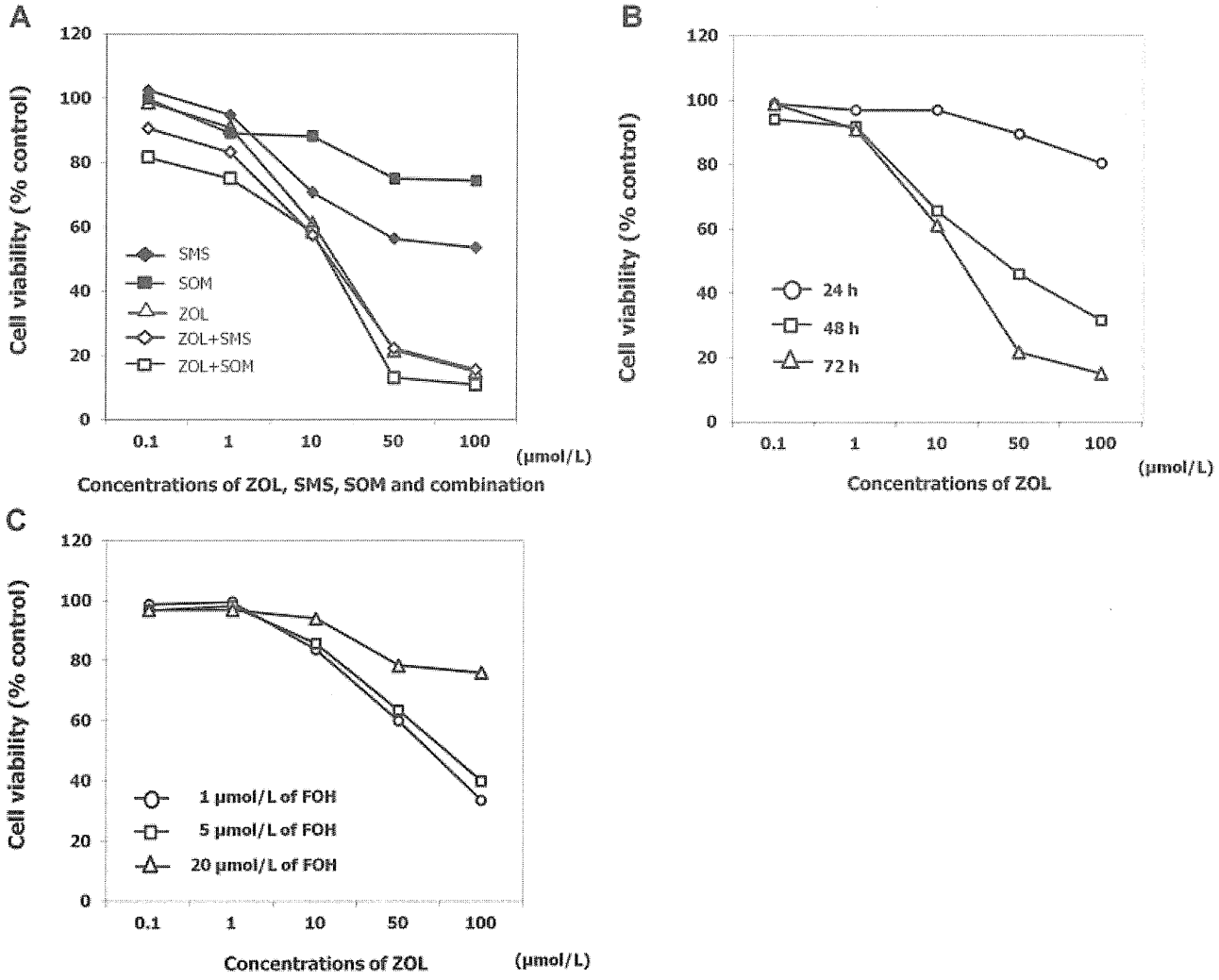

Fig. 3. Effects of ZOL, SMS and SOM as single agents and in combination on growth of NE-CS cells. Cell viability was measured by WST-8 assay when NE-CS cells were treated with various concentrations of ZOL, SMS and SOM (0.1–100 μmol/L) for 24, 48 or 72 hr. For combination, the same concentrations of ZOL and SMS or SOM were used. Cell viability was also measured when NE-CS cells were treated for 48 hr with the indicated concentrations (from 0.1 to 100 μmol/L) of ZOL plus 1, 5, and 20 μmol/L of farnesyl-pyrophosphate ammonium salt (FOH) (n = 5/group). **A**: Cell viability of NE-CS cells at 72 hr in each treatment group. The IC50 of ZOL at 72 hr for NE-CS cells was 15.7 μmol/L for ZOL, whereas it was 14.1 μmol/L for ZOL plus SMS, and 13.5 μmol/L for ZOL plus SOM. The combination of ZOL and somatostatin analogs did not create synergistic effects. **B**: Cell viability of NE-CS cells in time- and dose-dependent manners. ZOL induced time- and dose-dependent proliferative inhibition of NE-CS cells. **C**: Cell viability of NE-CS cells at 48 hr in ZOL plus FOH. ZOL-induced inhibition was reversed by 20 μmol/L of FOH.

concentrations of 0, 10, 50, and 100 μmol/L. The AI was significantly increased in ZOL 50, and 100 μmol/L compared to the control (means: 55.7 and 136.5, respectively, vs. 13.8) (Fig. 4B). The KI was significantly decreased in ZOL 10, 50, and 100 μmol/L compared to the control (means: 37.6, 22.8, and 1.3, respectively, vs. 68.7) (Fig. 4C).

ZOL Inhibits Migration of NE-CS Cells

In addition to effects of ZOL on cell cycle activity and apoptosis, we examined whether ZOL inhibited migration of NE-CS cells, using a Boyden chamber assay. NE-CS cells, with or without ZOL concentrations of 10, and 100 μmol/L, that migrated across the pores at 2, 4, 6 and 8 hr were counted. The numbers of cells migrating 1 mm^{-2} of membrane were significantly decreased in ZOL 10, and 100 μmol/L (Fig. 5A). When culture medium adding 20 μmol/L of FOH was incubated in upper chamber, the ZOL-induced inhibition was not appeared (Fig. 5B).

ZOL Utilizes the Ras/MAPK Pathway via the Mevalonate Pathway in NE-CS Cells

Since ZOL inhibits farnesyl-pyrophosphate synthetase in the mevalonate pathway and impairs prenylation of Ras, we evaluated the effects of ZOL on Ras activity. We used FOH, which potentially induces farnesylation of Ras. As evaluated by pull-down assay, 10, and 100 μmol/L inhibited Ras activation in NE-CS cells, and then the ZOL-induced inhibition was reversed by FOH (Fig. 6). We examined the effects of ZOL on Erk-1/2, which are the terminal proteins of the Ras/MAPK pathway. ZOL inhibited Erk1/2 phosphorylation as evaluated by Western blot assay.

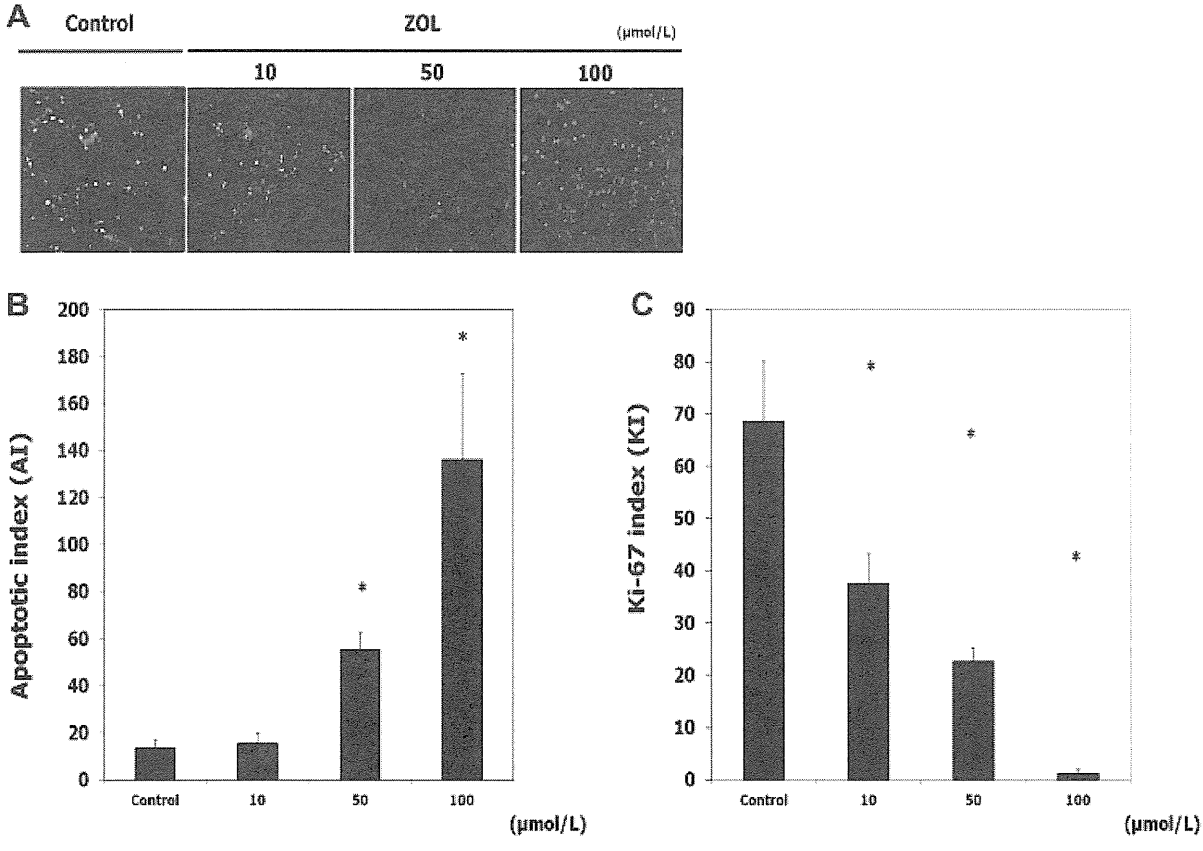

Fig. 4. Effects of ZOL on apoptosis and cell activity of NE-CS cells. **A**: TUNEL and anti-Ki67 immunofluorescence were used for NE-CS cells treated with ZOL concentrations of 0, 10, 50, and 100 μmol/L (n = 5/group). DAPI was used to visualize cell nuclei. TUNEL-positive cells, colored red, increased with increased concentrations of ZOL. On the other hand, Ki-67-positive cells, colored green, decreased. **B**: The numbers of TUNEL-positive cells per 1,000 cells apoptoic index (AI) were significantly increased in ZOL 50, and 100 μmol/L compared to the control (means: 55.7, and 136.5, respectively, vs. 13.8). Data are means; bars ± SD; *, significantly different from control group ($P < 0.001$; Student's *t*-test). **C**: The numbers of Ki67-positive cells per 1,000 cells (KI: Ki-67 labeling index) were significantly decreased in ZOL 10, 50, and 100 μmol/L compared to the control (means: 37.6, 22.8, and 1.3, respectively, vs. 68.7). Data are means; bars ± SD; *, significantly different from control group ($P < 0.001$; Student's *t*-test).

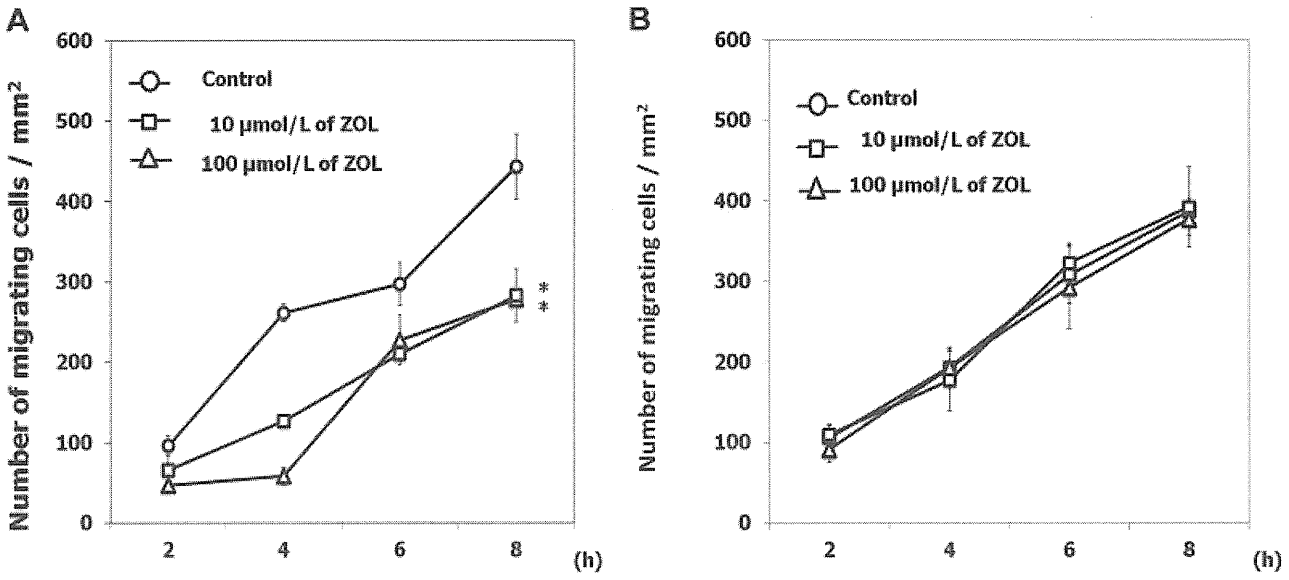

Fig. 5. Effects of ZOL on migration of NE-CS cells. Migration assay was performed by using a Boyden chamber (n = 3/group). **A**: In experiment 1, NE-CS cells (1×10^5) were placed in the upper chamber with 100 μl of culture medium with or without ZOL (10, 100 μmol/L). In the lower chamber, 600 μl of culture medium was added. The numbers of cells migrating per 1 mm^{-2} of membrane were significantly decreased in ZOL 10, and 100 μmol/L. Data are means; bars ± SD; *, significantly different from the control ($P < 0.001$; repeated-measures ANOVA). B: In experiment 2, culture medium adding 20 μmol/L of farnesyl-pyrophosphate ammonium salt (FOH) was incubated in the upper chamber. The numbers of cells migrating 1 mm^{-2} of membrane were not significantly decreased in ZOL 10, and 100 μmol/L. Data are means; bars ± SD. *, Significantly different from the control ($P < 0.001$; repeated-measures ANOVA).

DISCUSSION

Inappropriate NE regulation in the prostate might facilitate carcinogenesis, proliferation and other tissue changes such as loss of basal cells, angiogenesis, and piling up of prostatic luminal epithelium and invasion, which are characteristic of prostatic carcinoma [20]. In addition, we previously demonstrated that secretions from NE cells stimulated prostatic cancer cells to achieve androgen-independent growth [21]. Androgen deprivation therapy induces an increased number of NE cells in prostate cancer and the frequency and density of NE cells are more pronounced in CRPC [22]. Thus, the control of NE cells might be important for establishing a treatment strategy for CRPC.

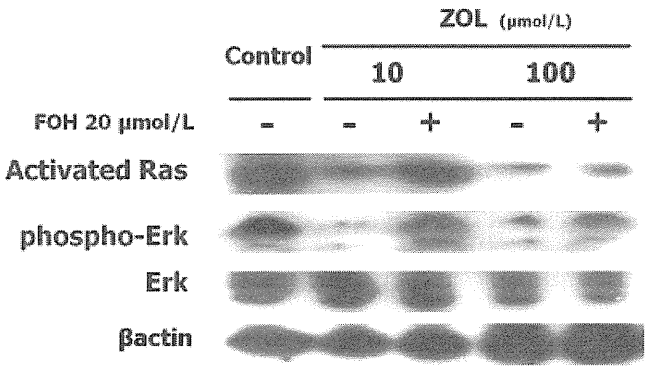

Fig. 6. Effects of ZOL on Ras/MAPK pathway of NE-CS cells. We used farnesyl-pyrophosphate ammonium salt (FOH), which potentially induces farnesylation of Ras. Ras activity was evaluated by pull-down assay, and Erk activity by Western blot assay. As evaluated by pull-down assay, 10, and 100 μmol/L ZOL inhibited Ras activation in NE-CS cells, and then the ZOL-induced inhibition was reversed by FOH. ZOL inhibited Erk1/2 phosphorylation in NE-CS cells as evaluated by Western blot assay.

Somatostatin analogs have been used clinically used to treat NE tumors [23]. SMS and lanreotide, which have high affinity to SSTR2a, have been demonstrated to reduce excessive hormone production and accompanying symptoms from carcinoid tumors and pancreatic endocrine tumors such as glucagonoma, VIPoma and gastrinoma [14]. The anticancer effect may be the result of antiproliferative and apoptoic actions through direct and indirect mechanisms. The direct mechanism is mediated by SSTR on tumor cells, and suppression of secretion of several growth factors such as insulin-like growth factor-1 (IGF-1) may also indirectly inhibit the tumor growth [24–26]. In this study, in spite of the expression of SSTR2a and SSTR5 in our NE carcinoma models, we failed to find significant antiproliferative effects of SMS or SOM monotherapy in vitro or in vivo. In addition, the combination therapy with ZOL did not create a synergistic effect. Although, the exact reason is unclear, both

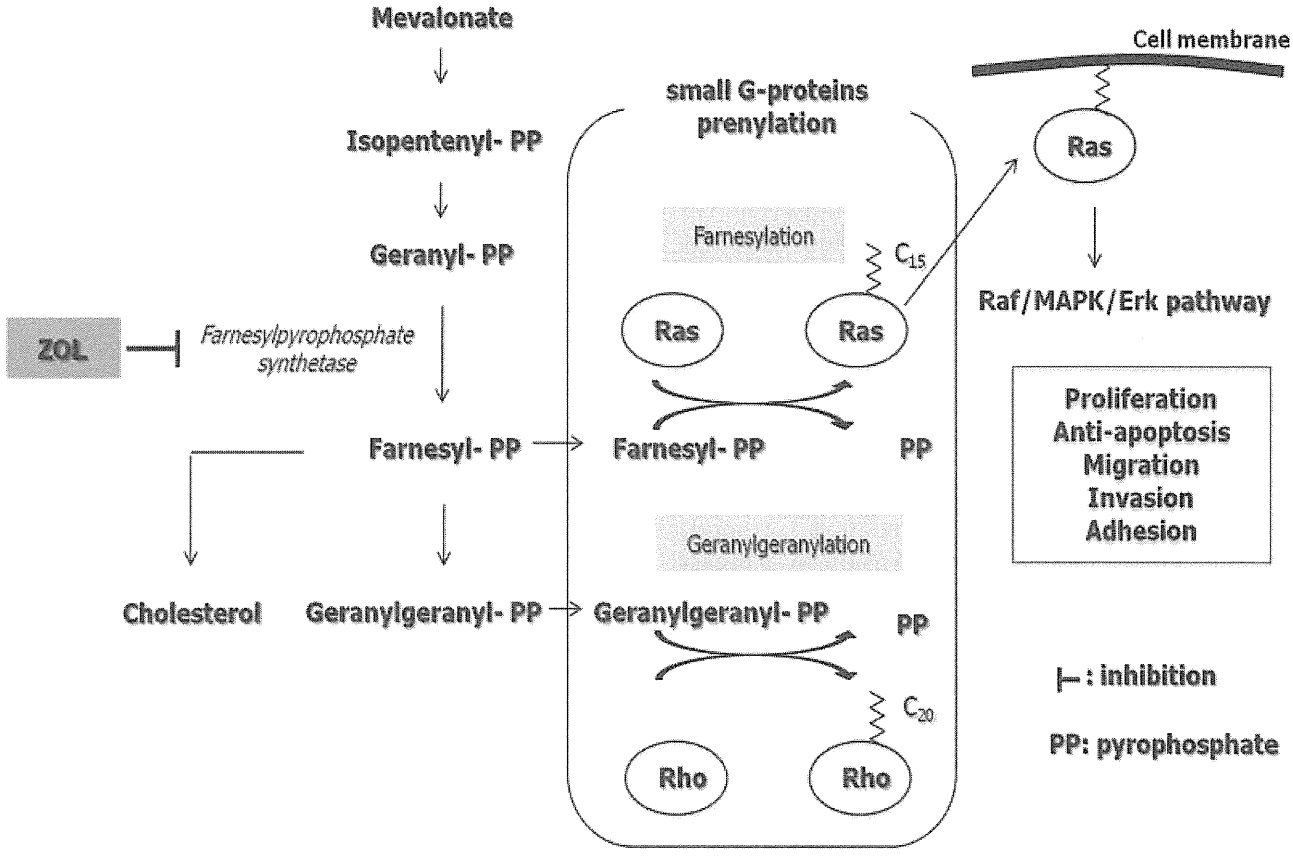

Fig. 7. Schematic representation of the mevalonate pathway and proposed mechanism of anti-tumor effects of zoledronic acid in prostatic NE carcinoma.

SMS and SOM might be insufficient to control our NE carcinoma models through autocrine, paracrine and endocrine regulation via SSTRs.

Our results suggest that ZOL induces time- and dose-dependent antiproliferative and apoptoic effects in prostatic NE carcinoma. The observed anticancer activity was exerted at ZOL IC50 levels of from 15.8 to 36.0 μmol/L. In addition, the drug reduced migration by 8 hr in vitro even at the 10 μmol/L concentration, and the time and dose did not seem to affect the viability of cells. These effects were caused by disruption of prenylation of Ras proteins as a result of farnesyl-pyrophosphate synthetase inhibition, disrupting the downstream MAPK/Erk signaling pathway (Fig. 7). Farnesyl-pyrophosphate synthetase is a key enzyme in the mevalonate pathway, which produces essential lipid molecules such as cholesterol, farnesyl-pyrophosphate and geranylgeranyl-pyrophosphate [27]. Small G proteins need prenylation to link to the inner surface of the cell membrane and function in signal translation [28]. Prenylation of small G proteins involves farnesylation, which provides a 15-carbon isoprenoid moiety with Ras, and geranylgeranylation, which provides a 20-carbon isoprenoid moiety with Rap Rac or Rho [27,28]. Ras is the most thoroughly characterized member of the small G proteins involved in key oncogenic cellular processes such as proliferation, anti-apoptosis, migration, invasion and adhesion (Fig. 7). Therefore, it is anticipated that ZOL disturbing prenylation of Ras will induce multifactorial anticancer effects in cancer cells.

Several studies had shown that ZOL induces apoptosis via impaired prenylation of small G proteins in various cancer cells, including prostate [12,29–31], breast [32,33], myeloma [34], colon [35], and lung cancer cell lines [36]. Caraglia et al. [12] reported the effects of the combination of ZOL and farnesyl-transferase inhibitor R115777 on PC3 and DU145 prostate cancer cell lines. These effects paralleled disruption of Ras/MAPK/Erk and Akt survival pathways, which consequently decreased phosphorylation of both mitochondrial bcl-2 and bad proteins, and caspase activation. These findings may support our results indicating that ZOL induced apoptosis of NE cells. Recents studies have shown that impaired geranylgeranylation on other small G proteins such as Rap1 [29,34] and RhoA [32] is also crucial for the association with these apoptotic actions induced by ZOL.

We also demonstrated that ZOL induced cell cycle arrest of the NE carcinoma cells. Both in vitro, and in

vivo, ZOL reduced the numbers of Ki67-positive cells during all active phases of the cell cycle (G1, S, G2, and M). ZOL has been shown to reduce the expression of cyclin D1 and cyclin E in osteosarcoma cells, resulting in a cell cycle block at G1, and S [37]. In addition, experiments using leukemia cells have shown that ZOL can also reduce the expression of cyclin D3 and cyclin B, resulting in a cell cycle block at G2-M [38]. These actions are suggested to occur in a p53-independent manner followed by subsequent apoptosis. Our results indicated that ZOL inhibited the cell cycle of NE cells.

Moreover, we demonstrated that ZOL inhibited migration of NE-CS cells. It decreased the weights of livers having metastatic nodules in castrated NE-10 allografts, which means to suppress liver metastases. Likewise, Hiraga et al. [39] reported that 1 μmol/L ZOL significantly inhibited cell invasion in a breast cancer cell line (4T1/Luc), which consequently led to suppression of liver and bone metastases. Similar results were also observed in prostate cancer cell lines LNCaP, PC3, and DU145 31. In addition, Coxon et al. [40] reported an inhibitory effect of 1 μmol/L ZOL on adhesion to mineralized matrix in PC3, and DU145 cells. Although the exact mechanisms underlying these effects remain unclear, it is suggested that ZOL could inhibit several matrix metalloproteinase or adhesion molecules via impairment of prenylation of small G proteins. It is noteworthy that ZOL also inhibits essential steps for the spread of cancer cells. In addition, recent reports have shown that ZOL indirectly exerts anticancer effects via elevated function of gamma delta T cells [41,42]. It is suggested that accumulation of isopentenyl-pyrophosphate caused by ZOL may be involved in activation of gamma delta T cells [43].

There are some limitations in this study. The NE-10 allograft and the NE-CS cell line were derived from the mouse prostate. The role of human NE cells in human prostate cancer may be different from that of mouse NE cells. In addition, the characteristics of the established cell line, NE-CS, could be different from those of the original NE-10 allograft because cells suitable for survival in vitro were selected during establishment of the cell line. However, there are no ideal human lines for which both in vitro, and in vivo NE carcinoma models are available. In addition, the concentration of ZOL that induced anticancer effects in our experiments was high in comparison to the peak plasma levels (393 ± 100 ng/ml) usually achieved by intravenous infusion in patients [44]. Anticancer effects of ZOL might be considered to be exerted basically in bone metastatic lesions in which high concentrations of ZOL are achieved.

In patients with bone metastasis of prostate cancer, ZOL is commonly used for relieving pain and preventing skeletal-related events. This study revealed effects of ZOL on NE cells, potential triggers of prostate cancer leading to CRPC. Regulating the microenvironment between NE cells and prostate cancer cells may result in benefits to patients who do not have clinically detected bone metastasis. We believe that our results support the clinical rationale for earlier proactive use of ZOL, though further studies will be needed to confirm this.

CONCLUSION

We examined the in vitro, and in vivo anti-tumor effects of ZOL and somatostatin analogs (SMS and SOM) on NE carcinoma models. Our results indicate that ZOL, but not SMS or SOM, induces apoptosis and inhibition of proliferation and migration through impaired prenylation of Ras. Our findings support the possibility that ZOL could be used in the early phase for controlling NE cells which may trigger progression of prostate cancer to CRPC.

REFERENCES

1. Jemal A, Bray F, Center MM, Ferlay J, Ward E, Forman D. Global cancer statistics. CA Cancer J Clin 2011;61(2):69–90.
2. Heidenreich A, Aus G, Bolla M, Joniau S, Matveev VB, Schmid HP, Zattoni F. EAU guidelines on prostate cancer. Eur Urol 2008;53(1):68–80.
3. Debes JD, Tindall DJ. Mechanisms of androgen-refractory prostate cancer. N Engl J Med 2004;351(15):1488–1490.
4. di Sant'Agnese PA. Neuroendocrine differentiation in prostatic carcinoma: An update. Prostate Suppl 1998;8:74–79.
5. Ito T, Yamamoto S, Ohno Y, Namiki K, Aizawa T, Akiyama A, Tachibana M. Up-regulation of neuroendocrine differentiation in prostate cancer after androgen deprivation therapy, degree and androgen independence. Oncol Rep 2001;8(6): 1221–1224.
6. Hirano D, Okada Y, Minei S, Takimoto Y, Nemoto N. Neuroendocrine differentiation in hormone refractory prostate cancer following androgen deprivation therapy. Eur Urol 2004;45(5): 586–592; discussion 592.
7. Masumori N, Thomas TZ, Chaurand P, Case T, Paul M, Kasper S, Tsukamoto T, Shappell SB, Matusik RJ. A probasin–Large T antigen transgenic mouse line develops prostate adenocarcinoma and neuroendocrine carcinoma with metastatic potential. Cancer Res 2001;61(5):2239–2249.
8. Masumori N, Tsuchiya K, Tu WH, Lee C, Kasper S, Tsukamoto T, Shappell SB, Matusik RJ. An allograft model of androgen independent prostatic neuroendocrine carcinoma derived from a large probasin promoter-T antigen transgenic mouse line. J Urol 2004;171(1):439–442.
9. Uchida K, Masumori N, Takahashi A, Itoh N, Tsukamoto T. Characterization of prostatic neuroendocrine cell line established from neuroendocrine carcinoma of transgenic mouse allograft model. Prostate 2005;62(1):40–48.

10. Uchida K, Masumori N, Takahashi A, Itoh N, Kato K, Matusik RJ, Tsukamoto T. Murine androgen-independent neuroendocrine carcinoma promotes metastasis of human prostate cancer cell line LNCaP. Prostate 2006;66(5):536–545.
11. Saad F, Gleason DM, Murray R, Tchekmedyian S, Venner P, Lacombe L, Chin JL, Vinholes JJ, Goas JA, Chen B. A randomized, placebo-controlled trial of zoledronic acid in patients with hormone-refractory metastatic prostate carcinoma. J Natl Cancer Inst 2002;94(19):1458–1468.
12. Caraglia M, Marra M, Leonetti C, Meo G, D'Alessandro AM, Baldi A, Santini D, Tonini G, Bertieri R, Zupi G, Budillon A, Abbruzzese A. R115777 (Zarnestra)/Zoledronic acid (Zometa) cooperation on inhibition of prostate cancer proliferation is paralleled by Erk/Akt inactivation and reduced Bcl-2 and bad phosphorylation. J Cell Physiol 2007;211(2):533–543.
13. Patel YC. Somatostatin its receptor, family Front Neuroendocrinol 1999;20(3):157–198.
14. Hejna M, Schmidinger M, Raderer M. The clinical role of somatostatin analogs as antineoplastic agents: Much ado about nothing? Ann Oncol 2002;13(5):653–668.
15. Reubi JC, Waser B, Schaer JC, Laissue JA. Somatostatin receptor SSTR1–SSTR5 expression in normal and neoplastic human tissues using receptor autoradiography with subtype-selective ligands. Eur J Nucl Med 2001;28(7):836–846.
16. Halmos G, Schally AV, Sun B, Davis R, Bostwick DG, Plonowski A. High expression of somatostatin receptors and messenger ribonucleic acid for its receptor subtypes in organ-confined and locally advanced human prostate cancers. J Clin Endocrinol Metab 2000;85(7):2564–2571.
17. Bruns C, Lewis I, Briner U, Meno-Tetang G, Weckbecker G. SO M230 a novel somatostatin peptidomimetic with broad somatotropin release inhibiting factor (SRIF) receptor binding and a unique antisecretory profile. Eur J Endocrinol 2002 ;146(5):707–716.
18. Chou TC, Talalay P. Quantitative analysis of dose-effect relationships: The combined effects of multiple drugs or enzyme inhibitors. Adv Enzyme Regul 1984;22:27–55.
19. Topaly J, Zeller WJ, Fruehauf S. Synergistic activity of the new ABL-specific tyrosine kinase inhibitor STI571 and chemotherapeutic drugs on BCR-ABL-positive chronic myelogenous leukemia cells. Leukemia 2001;15(3):342–347.
20. Bok RA, Small EJ. Bloodborne biomolecular markers in prostate cancer development and progression. Nat Rev Cancer 2002;2(12):918–926.
21. Jin RJ, Wang Y, Masumori N, Ishii K, Tsukamoto T, Shappell SB, Hayward SW, Kasper S, Matusik RJ. NE-10 neuroendocrine cancer promotes the LNCaP xenograft growth in castrated mice. Cancer Res 2004;64(15):5489–5495.
22. Weinstein MH, Partin AW, Veltri RW, Epstein JI. Neuroendocrine differentiation in prostate cancer: Enhanced prediction of progression after radical prostatectomy. Hum Pathol 1996; 27(7):683–687.
23. Sciarra A, Bosman C, Monti G, Gentile V, Autran Gomez AM, Ciccariello M, Pastore A, Salvatori G, Fattore F, Di Silverio F. Somatostatin analogs and estrogens in the treatment of androgen ablation refractory prostate adenocarcinoma. J Urol 2004;172(5 Pt 1):1775–1783.
24. Pawlikowski M, Melen-Mucha G. Perspectives of new potential therapeutic applications of somatostatin analogs. Neuro Endocrinol Lett 2003;24(1–2):21–27.
25. van der Hoek J, van der Lelij AJ, Feelders RA, de Herder WW, Uitterlinden P, Poon KW, Boerlin V, Lewis I, Krahnke T, Hofland LJ, Lamberts SW. The somatostatin analogue SOM230, compared with octreotide, induces differential effects in several metabolic pathways in acromegalic patients. Clin Endocrinol (Oxf) 2005;63(2):176–184.
26. Schmid HA. Pasireotide (SOM230): Development, mechanism of action and potential applications. Mol Cell Endocrinol 2008;286(1–2):69–74.
27. Kavanagh KL, Guo K, Dunford JE, Wu X, Knapp S, Ebetino FH, Rogers MJ, Russell RG, Oppermann U. The molecular mechanism of nitrogen-containing bisphosphonates as antiosteoporosis drugs. Proc Natl Acad Sci USA 2006;103(20):7829–7834.
28. Hougland JL, Fierke CA. Getting a handle on protein prenylation. Nat Chem Biol 2009;5(4):197–198.
29. Nogawa M, Yuasa T, Kimura S, Kuroda J, Segawa H, Sato K, Yokota A, Koizumi M, Maekawa T. Zoledronic acid mediates Ras-independent growth inhibition of prostate cancer cells. Oncol Res 2005;15(1):1–9.
30. Fabbri F, Brigliadori G, Carloni S, Ulivi P, Vannini I, Tesei A, Silvestrini R, Amadori D, Zoli W. Zoledronic acid increases docetaxel cytotoxicity through pMEK and Mcl-1 inhibition in a hormone-sensitive prostate carcinoma cell line. J Transl Med 2008;6:43.
31. Mani J, Vallo S, Barth K, Makarevic J, Juengel E, Bartsch G, Wiesner C, Haferkamp A, Blaheta RA. Zoledronic acid influences growth, migration and invasive activity of prostate cancer cells in vitro. Prostate Cancer Prostatic Dis 2012;15(3):250–255.
32. Denoyelle C, Hong L, Vannier JP, Soria J, Soria C. New insights into the actions of bisphosphonate zoledronic acid in breast cancer cells by dual RhoA-dependent and -independent effects. Br J Cancer 2003;88(10):1631–1640.
33. Ottewell PD, Lefley DV, Cross SS, Evans CA, Coleman RE, Holen I. Sustained inhibition of tumor growth and prolonged survival following sequential administration of doxorubicin and zoledronic acid in a breast cancer model. Int J Cancer 2009;126(2):522–532.
34. Guenther A, Gordon S, Tiemann M, Burger R, Bakker F, Green JR, Baum W, Roelofs AJ, Rogers MJ, Gramatzki M. The bisphosphonate zoledronic acid has antimyeloma activity in vivo by inhibition of protein prenylation. Int J Cancer 2010;126(1):239–246.
35. Sewing L, Steinberg F, Schmidt H, Goke R. The bisphosphonate zoledronic acid inhibits the growth of HCT-116 colon carcinoma cells and induces tumor cell apoptosis. Apoptosis 2008; 13(6):782–789.
36. Tannehill-Gregg SH, Levine AL, Nadella MV, Iguchi H, Rosol TJ. The effect of zoledronic acid and osteoprotegerin on growth of human lung cancer in the tibias of nude mice. Clin Exp Metast 2006;23(1):19–31.
37. Kubista B, Trieb K, Sevelda F, Toma C, Arrich F, Heffeter P, Elbling L, Sutterluty H, Scotlandi K, Kotz R, Micksche M, Berger W. Anticancer effects of zoledronic acid against human osteosarcoma cells. J Orthop Res 2006;24(6):1145–1152.
38. Kuroda J, Kimura S, Segawa H, Kobayashi Y, Yoshikawa T, Urasaki Y, Ueda T, Enjo F, Tokuda H, Ottmann OG, Maekawa T. The third-generation bisphosphonate zoledronate synergistically augments the anti-pH + leukemia activity of imatinib mesylate. Blood 2003;102(6):2229–2235.
39. Hiraga T, Williams PJ, Ueda A, Tamura D, Yoneda T. Zoledronic acid inhibits visceral metastases in the 4T1/Luc mouse breast cancer model. Clin Cancer Res 2004;10(13):4559–4567.